

# pyUserCalc: A revised Jupyter notebook calculator for uranium-series disequilibria in basalts

Elkins, Lynne J.<sup>1</sup> and Spiegelman, Marc<sup>2</sup>

<sup>1</sup>*University of Nebraska-Lincoln, Lincoln, NE, USA, lelkins@unl.edu*

<sup>2</sup>*Lamont-Doherty Earth Observatory of Columbia University, Palisades, NY, USA, mspieg@ldeo.columbia.edu*

## Abstract

Meaningful analysis of uranium-series isotopic disequilibria in basaltic lavas relies on the use of complex forward numerical models like dynamic melting (McKenzie, 1985) and equilibrium porous flow (Spiegelman and Elliott, 1993). Historically, such models have either been solved analytically for simplified scenarios, such as constant melting rate or constant solid/melt trace element partitioning throughout the melting process, or have relied on incremental or numerical calculators with limited power to solve problems and/or restricted availability. The most public numerical solution to reactive porous flow, UserCalc (Spiegelman, 2000) was maintained on a private institutional server for nearly two decades, but that approach has been unsustainable in light of modern security concerns. Here we present a more long-lasting solution to the problems of availability, model sophistication and flexibility, and long-term access in the form of a cloud-hosted, publicly available Jupyter notebook. Similar to UserCalc, the new notebook calculates U-series disequilibria during time-dependent, equilibrium partial melting in a one-dimensional porous flow regime where mass is conserved. In addition, we also provide a new disequilibrium transport model which has the same melt transport model as UserCalc, but approximates rate-limited diffusive exchange of nuclides between solid and melt using linear kinetics. The degree of disequilibrium during transport is controlled by a Damköhler number, allowing the full spectrum of equilibration models from complete fractional melting ( $Da = 0$ ) to equilibrium transport ( $Da = \infty$ ).

## Key Points

- Cloud-based Jupyter notebook presents an open source, reproducible tool for modeling U-series in basalts
- Equilibrium and pure disequilibrium porous flow U-series models with 1D conservation of mass
- Scaled porous flow model introduces incomplete equilibrium scenario with reaction rate limitations

## 1 Introduction

Continuous forward melting models are necessary to interpret the origins of empirically-measured U-series isotopic disequilibria in basaltic lavas, but the limited and unreliable availability of reproducible tools for making such calculations remains a persistent problem for geo-

36 chemists. To date, a number of models have been developed for this task, including classical  
37 dynamic melting after McKenzie (1985) and the reactive porous flow model of Spiegelman and  
38 Elliott (1993). There have since been numerous approaches to using both the dynamic and porous  
39 flow models that range from simplified analytical solutions (e.g., Sims et al., 1999; Zou, 1998; Zou  
40 and Zindler, 2000) to incremental dynamic melting calculators (Stracke et al., 2003), two-porosity  
41 calculators (Jull et al., 2002; Lundstrom et al., 2000; Sims et al., 2002), and one-dimensional numer-  
42 ical solutions to reactive porous flow (Spiegelman, 2000) and dynamic melting (Bourdon et al.,  
43 2005; Elkins et al., 2019). Unfortunately, some of the approaches published since 1990 lacked pub-  
44 licly available tools that would permit others to directly apply the authors' methods, and while  
45 the more simplified and incremental approaches remain appropriate for asking and approaching  
46 some questions, they are insufficient for other applications that require more complex approaches  
47 (e.g., two-lithology melting; Elkins et al., 2019). Other tools like UserCalc that were available to  
48 public users (Spiegelman, 2000) were limited in application and have since become unavailable.

49 In light of the need for more broadly accessible and flexible solutions to U-series disequilibrium  
50 problems in partial melting, here we present a cloud-server hosted, publicly available numerical  
51 calculator for one-dimensional, decompression partial melting. The tool is provided in a Jupyter  
52 notebook with importable Python code and can be accessed from a web browser. Users will be  
53 able to access and use the tool using a free cloud server account, or on their own computer given  
54 any standard Python distribution. As shown below, the notebook is structured to permit the user  
55 to select one of two primary model versions, either classical reactive porous flow after Spiegelman  
56 and Elliott (1993) and Spiegelman (2000), or a new disequilibrium transport model, developed af-  
57 ter the appendix formulas of Spiegelman and Elliott (1993). The new model ranges from pure  
58 disequilibrium porous flow transport (i.e., the mass-conserved equivalent of true fractional melt-  
59 ing over time) to a "scaled" disequilibrium scenario, where the degree of chemical equilibrium  
60 that is reached is determined by the relationship between the rate of chemical reaction and the  
61 solid decompression rate (which is, in turn, related to the overall melting rate), in the form of a  
62 Damköhler number.

63 This scaled disequilibrium model resembles the classic dynamic melting model of McKenzie  
64 (1985), with the caveat that ours is the first U-series melting model developed for near-fractional,  
65 disequilibrium transport where mass is also conserved within a one-dimensional melting regime.  
66 That is, rather than controlling the quantity of melt that remains in equilibrium with the solid  
67 using a fixed residual porosity, the melt porosity is controlled by Darcy's Law and mass conserva-  
68 tion constraints after Spiegelman and Elliott (1993), and the "near-fractional" scenario is simulated  
69 using the reaction rate of the migrating liquid with the upwelling solid matrix.

## 70 **2 Calculating U-series in basalts during mass-conserved, one-** 71 **dimensional porous flow**

### 72 **2.1 Solving for equilibrium transport**

73 Here we consider several forward melting models that calculate the concentrations and activities  
74 of U-series isotopes ( $^{238}\text{U}$ ,  $^{230}\text{Th}$ ,  $^{226}\text{Ra}$ ,  $^{235}\text{U}$ , and  $^{231}\text{Pa}$ ) during partial melting and melt transport  
75 due to adiabatic mantle decompression. Following Spiegelman and Elliott (1993), we start with  
76 conservation of mass equations for the concentration of a nuclide  $i$ , assuming chemical equilib-  
77 rium between melt and solid:

$$\frac{\partial}{\partial t}[\rho_f\phi + \rho_s(1 - \phi)D_i]c_i^f + \nabla \cdot [\rho_f\phi v + \rho_s(1 - \phi)D_iV]c_i^f = \lambda_{i-1}[\rho_f\phi + \rho_s(1 - \phi)D_{i-1}]c_{i-1}^f - \lambda_i[\rho_f\phi + \rho_s(1 - \phi)D_i]c_i^f \quad (1)$$

78 where  $t$  is time,  $c_i^f$  is the concentration of nuclide  $i$  in the melt,  $D_i$  is the bulk solid/liquid partition  
 79 coefficient for nuclide  $i$ ,  $\rho_f$  is the density of the fluid and  $\rho_s$  is the density of the solid,  $\phi$  is the  
 80 maximum residual melt porosity,  $v$  is the velocity of the melt and  $V$  the velocity of the solid in  
 81 three dimensions,  $\lambda_i$  is the decay constant of nuclide  $i$ , and  $(i - 1)$  indicates the radioactive parent  
 82 of nuclide  $i$ . Equation (1) states that the change in total mass of nuclide  $i$  in both the melt and  
 83 the solid is controlled by the divergence of the mass flux transported by both phases and by the  
 84 radioactive decay of both parent and daughter nuclides (i.e., the right hand side of the equation  
 85 above).

86 The equilibrium model of Spiegelman and Elliott (1993) assumes complete chemical equilibrium  
 87 is maintained between the migrating partial melt and the solid rock matrix along a decompressing  
 88 one-dimensional column. To close the equations, they assume that melt transport is described by a  
 89 simplified form of Darcy's Law for permeable flow through the solid matrix. In one dimension, for  
 90 a steady-state upwelling column of melting mantle rocks, they defined the one-dimensional melt  
 91 and solid velocities ( $w$  and  $W$ , respectively), and expressed the melt and solid fluxes as functions  
 92 of height ( $z$ ) in terms of a constant melting rate  $\Gamma_0$ :

$$\rho_f\phi w = \Gamma_0 z \quad (2)$$

$$\rho_s(1 - \phi)W = \rho_s W_0 - \Gamma_0 z \quad (3)$$

93 where  $W_0$  is the solid mantle upwelling rate, and  $\Gamma_0$  is equivalent to  $\rho_s W_0 F_{max}$  divided by the depth  
 94  $d$  for a maximum degree of melting  $F_{max}$ .

95 Assuming an initial condition of secular equilibrium, where the initial activities  $\lambda_i c_{i,0}^f D_i$  are equiv-  
 96 alent for parent and daughter nuclides, they derived a system of differential equations for the  
 97 concentration  $c_i^f$  in any decay chain, which can be solved numerically using equation (10) from  
 98 that paper:

$$\frac{dc_i^f}{d\zeta} = c_i^f \frac{(D_i - 1)F_{max}}{D_i + (1 - D_i)F_{max}\zeta} + \lambda_i d \left[ \frac{D_i[D_{i-1} + (1 - D_{i-1})F_{max}\zeta]}{D_{i-1}[D_i + (1 - D_i)F_{max}\zeta]} \frac{c_{i-1}^f}{w_{eff}^{i-1}} - \frac{c_i^f}{w_{eff}^i} \right] \quad (4)$$

99 where  $c_i^f$  is the scaled melt concentration ( $= c_i^f / c_{i,0}^f$ ),  $\zeta$  is the dimensionless fractional height in the  
 100 scaled column, equal to 0 at the base and 1 at the top, and

$$w_{eff}^i = \frac{\rho_f\phi w + \rho_s(1 - \phi)D_i W}{\rho_f\phi + \rho_s(1 - \phi)D_i} \quad (5)$$

101 is the effective velocity for element  $i$ .

102 In their appendix, Spiegelman and Elliott (1993) developed the more general (and, arguably, realis-  
 103 tic) form where  $\Gamma$  and  $D_i$  are functions of height  $z$ . The UserCalc model of Spiegelman (2000) then  
 104 formulated a one-dimensional numerical integration for the concentrations of selected U-series  
 105 isotopes in continuously produced partial melts with height  $z$ , after the equilibrium formulas  
 106 above. The concentration expression derived by Spiegelman (2000) for the equilibrium scenario  
 107 (formula 6 in that reference) is:

$$\frac{dc_i^f}{dz} = \frac{-c_i^f(z)}{F(z) + (1 - F(z))D_i(z)} \frac{d}{dz} [F(z) + (1 - F(z))D_i(z)] + \frac{\lambda_{i-1}\overline{\rho D_{i-1}}c_{i-1}^f(z) - \lambda_i\overline{\rho D_i}c_i^f(z)}{\rho_s W_0 [F(z) + (1 - F(z))D_i(z)]} \quad (6)$$

108 where  $F$  is the degree of melting. Spiegelman (2000) further observed that solving for the nat-  
 109 ural log of the concentrations,  $U_i$ , rather than the concentrations themselves, is more accurate,  
 110 particularly for highly incompatible elements (formulas 7-9 in that reference):

$$U_i^f = \ln \left( \frac{c_i^f}{c_{i,0}^f} \right) \quad (7)$$

$$\frac{dU_i^f}{dz} = \frac{1}{c_i^f(z)} \frac{dc_i^f}{dz} \quad (8)$$

$$\frac{dU_i^f}{dz} = \frac{-1}{F(z) + (1 - F(z))D_i(z)} \frac{d}{dz} [F(z) + (1 - F(z))D_i(z)] + \frac{\lambda_i}{w_{eff}^i} [R_i^{i-1} \exp[U_{i-1}^f(z) - U_i^f(z)] - 1] \quad (9)$$

111 For the formulas above, Spiegelman (2000) defined a series of variables that allow for simpler  
 112 integration formulas and aid in efficient solution of the model, namely

$$\overline{\rho D_i} = \rho_f \phi + \rho_s (1 - \phi) D_i(z), \quad (10)$$

$$\overline{F} = F(z) + (1 - F(z))D_i(z), \quad (11)$$

$$R_i^{i-1} = \alpha_i \frac{D_i^0 \overline{\rho D_{i-1}}}{D_{i-1}^0 \overline{\rho D_i}}, \quad (12)$$

$$\alpha_i = \frac{\lambda_{i-1} c_{(i-1),0}^s}{\lambda_i c_{i,0}^s}, \quad (13)$$

113 and substituting from the formulas above

$$w_{eff}^i = \frac{\rho_s W_0 \overline{F}}{\overline{\rho D_i}}. \quad (14)$$

114 where  $D_i^0$  is the initial bulk solid/melt partition coefficient for element  $i$ ,  $R_i^{i-1}$  is the ingrowth  
 115 factor, and  $\alpha$  is the initial degree of secular disequilibrium in the unmelted solid.

116  $U_i(z) = \ln(c_f(z)/c_f^0)$ , the log of the total concentration of nuclide  $i$  in the melt, can then be decom-  
 117 posed into

$$U_i(z) = U_i^{stable}(z) + U_i^{rad}(z) \quad (15)$$

118 where

$$U_i^{stable}(z) = \ln \left[ \frac{D_i^0}{\overline{FD}_i(z)} \right] \quad (16)$$

119 is the log concentration of a stable nuclide with the same partition coefficients, and  $U_i^{rad}(z)$  is the  
 120 radiogenic ingrowth component. An alternate way of writing the radiogenic ingrowth component  
 121 of equation (9) of Spiegelman (2000) is:

$$\frac{dU_i^{rad}}{dz} = \lambda'_i \frac{\overline{\rho D}_i}{\overline{FD}_i} \left[ R_i^{i-1} \exp[U_{i-1}(z) - U_i(z)] - 1 \right] \quad (17)$$

122 where

$$\lambda'_i = \frac{h\lambda_i}{W_0} \quad (18)$$

123 is the decay constant of nuclide  $i$ , scaled by the solid transport time ( $h/W_0$ ) across a layer of total  
 124 height  $h$ .

125 Using these equations, the UserCalc reactive porous flow calculator accepted user inputs for both  
 126  $F(z)$  and  $D_i(z)$ . The method uses a formula for the melt porosity ( $\phi(z)$ ) based on a Darcy's Law  
 127 expression with a scaled permeability factor (formula 20 from Spiegelman (2000)):

$$K_r(z) A_d \phi^n (1 - \phi)^2 + \phi [1 + F(z) \left( \frac{\rho_s}{\rho_f} - 1 \right)] - \frac{\rho_s}{\rho_f} F(z) = 0 \quad (19)$$

128 where  $K_r(z)$  is the scaled permeability with height  $z$ ,  $A_d$  is a permeability calibration function, and  
 129  $n$  is the permeability exponent. The scaled permeability is calculated relative to the permeability  
 130 at the top of the column, i.e. depth  $z = z_{final}$ :

$$K_r(z) = \frac{k(z)}{k(z_{final})} \quad (20)$$

131 Our model implementation reproduces and builds on the prior efforts summarized above, using  
 132 a readily accessible computer language (Python) and web application (Jupyter notebooks).

## 133 2.2 Solving for complete disequilibrium transport

134 We further present a calculation tool that solves a similar set of equations for pure chemical dis-  
 135 equilibrium transport during one-dimensional decompression melting. This model assumes that  
 136 the solid produces an instantaneous fractional melt in local equilibrium with the solid; how-  
 137 ever, the melt is not allowed to back-react with the solid during transport, as it would in the  
 138 equilibrium model above. In the limiting condition defined by stable trace elements (i.e., without  
 139 radioactive decay), the model reduces to the calculation for an accumulated fractional melt. The  
 140 model solves for the concentration of each nuclide  $i$  in the solid ( $s$ ) and liquid ( $f$ ) using equations  
 141 (26) and (27) of Spiegelman and Elliott (1993):

$$\frac{dc_i^s}{dz} = \frac{c_i^s(z)(1 - \frac{1}{D_i(z)})}{1 - F(z)} \frac{dF}{dz} + \frac{1 - \phi}{W_0(1 - F(z))} [\lambda_{i-1}c_{i-1}^s(z) - \lambda_i c_i^s(z)] \quad (21)$$

$$\frac{dc_i^f}{dz} = \frac{\frac{c_i^s(z)}{D_i(z)} - c_i^f(z)}{F(z)} \frac{dF}{dz} + \frac{\rho_f \phi}{\rho_s W_0 F(z)} [\lambda_{i-1}c_{i-1}^f(z) - \lambda_i c_i^f(z)] \quad (22)$$

142 which maintain conservation of mass for both fluid and solid individually, and do not assume  
 143 chemical equilibration between the two phases.

144 As above, the solid and fluid concentration equations are rewritten in terms of the logs of the  
 145 concentrations:

$$U_i^s(z) = \ln \left( \frac{c_i^s(z)}{c_{i,0}^s} \right), \quad U_i^f(z) = \ln \left( \frac{c_i^f(z)}{c_{i,0}^f} \right) \quad (23)$$

146 and thus

$$\frac{dU_i}{dz} = \frac{1}{c_i(z)} \frac{dc_i}{dz} \quad (24)$$

147 We assume that initial  $c_{i,0}^s = D_{i,0}c_{i,0}^f$ . Also as above, the log concentration equations can be broken  
 148 into stable and radiogenic components, and the stable log concentration equations are:

$$\frac{dU_i^{s,stable}}{dz} = \frac{1 - \frac{1}{D_i(z)}}{1 - F(z)} \frac{dF}{dz} \quad (25)$$

$$\frac{dU_i^{f,stable}}{dz} = \frac{\frac{D_i^0}{D_i(z)} \exp(U_i^s - U_i^f)}{F(z)} \quad (26)$$

149 Reincorporating this with the radiogenic component gives:

$$\frac{dU_i^s}{dz} = \frac{1 - \frac{1}{D_i(z)}}{1 - F(z)} \frac{dF}{dz} + \frac{1 - \phi}{1 - F(z)} \lambda_i \left[ \frac{\alpha_{i-1}}{\alpha_i} \exp[U_{i-1}^s - U_i^s] - 1 \right] \quad (27)$$

$$\frac{dU_i^f}{dz} = \frac{D_i^0}{D_i(z)} \frac{\exp(U_i^s - U_i^f)}{F(z)} + \frac{\rho_f \phi}{\rho_s F} \lambda_i \left[ \frac{D_i^0 \alpha_{i-1}}{D_{i-1}^0 \alpha_i} \exp[U_{i-1}^f - U_i^f] - 1 \right] \quad (28)$$

### 150 2.3 Solving for transport with chemical reactivity rates

151 The two models described above are end members for complete equilibrium and complete dis-  
 152 equilibrium transport. For stable trace elements, these models produce melt compositions that  
 153 are equivalent to batch melting and accumulated fractional melting (e.g., Spiegelman and Elliott,  
 154 1993). However, the actual transport of a reactive fluid (like a melt) through a solid matrix can fall  
 155 anywhere between these end members depending on the rate of transport and re-equilibration  
 156 between melt and solid, which can be sensitive to the mesoscopic geometry of melt and solid (e.g.,  
 157 Spiegelman and Kenyon, 1992). In an intermediate scenario, we envision that some reaction oc-  
 158 curs, but chemical equilibration is incomplete due to slow reaction rates relative to the differential  
 159 transport rates for the fluid and solid. If reaction times are sufficiently rapid to achieve chemical  
 160 exchange over the lengthscale of interest before the liquid segregates, chemical equilibrium can  
 161 be achieved; but for reactions that occur more slowly than effective transport rates, something  
 162 less than full equilibrium occurs (e.g., Grose and Afonso, 2019; Iwamori, 1993, 1994; Kogiso et al.,  
 163 2004; Liang and Liu, 2016; Peate and Hawkesworth, 2005; Qin et al., 1992). Such reaction rates  
 164 can include, for example, the rate of chemical migration over the distance between high porosity  
 165 veins or channels (e.g., Aharonov et al., 1995; Jull et al., 2002; Spiegelman et al., 2001; Stracke and  
 166 Bourdon, 2009); or, at the grain scale, the solid chemical diffusivity of elements over the diameter  
 167 of individual mineral grains (e.g., Feineman and DePaolo, 2003; Grose and Afonso, 2019; Oliveira  
 168 et al., 2020; Van Orman et al., 2002a, 2006).

169 To model this scaled reactivity scenario, here we start with our equations for disequilibrium trans-  
 170 port in a steady-state, one-dimensional conservative system, and add a chemical back-reaction  
 171 term that permits exchange of elements between the fluid and the solid. The reaction term is  
 172 scaled by a reactivity rate factor,  $\Re$  and expressed in  $\text{kg}/\text{m}^3/\text{yr}$ . (i.e., the same units as the melting  
 173 rate).

174 First, returning to the conservation of mass equations for a steady-state, one-dimensional, reactive  
 175 system of stable trace elements, and using  $\Gamma(z)$  to represent the melting rate:

$$\frac{d}{dz} \rho_f \phi w = \Gamma(z) \quad (29)$$

$$\frac{d}{dz} \rho_s (1 - \phi) W = -\Gamma(z) \quad (30)$$

$$\frac{d}{dz} \rho_f \phi w c_i^f(z) = \frac{c_i^s(z)}{D_i(z)} \Gamma(z) - \Re \left( c_i^f(z) - \frac{c_i^s(z)}{D_i(z)} \right) \quad (31)$$

$$\frac{d}{dz} \rho_s (1 - \phi) W c_i^s(z) = -\frac{c_i^s(z)}{D_i(z)} \Gamma(z) + \Re \left( c_i^f(z) - \frac{c_i^s(z)}{D_i(z)} \right) \quad (32)$$

176 where, for an adiabatic upwelling column,

$$\Gamma(z) = \rho_s W_0 \frac{dF}{dz} \quad (33)$$

177 From this, the equations (29) and (30) can be integrated (with appropriate boundary conditions at  
178  $z = 0$ ) to give

$$\rho_f \phi w = \rho_s W_0 F(z) \quad (34)$$

$$\rho_s (1 - \phi) W = \rho_s W_0 (1 - F(z)) \quad (35)$$

179 Next, we expand the concentration equations to include the reactivity factor, and substitute the  
180 conservation of total mass determined above:

$$\rho_s W_0 F(z) \frac{d}{dz} c_i^f(z) + c_i^f(z) \Gamma(z) = \frac{c_i^s(z)}{D_i(z)} \Gamma(z) - \Re \left( c_i^f(z) - \frac{c_i^s(z)}{D_i(z)} \right) \quad (36)$$

$$\rho_s W_0 (1 - F(z)) \frac{d}{dz} c_i^s(z) - c_i^s(z) \Gamma(z) = -\frac{c_i^s(z)}{D_i(z)} \Gamma(z) + \Re \left( c_i^f(z) - \frac{c_i^s(z)}{D_i(z)} \right) \quad (37)$$

181 If we then combine the  $\Gamma(z)$  terms and rearrange:

$$\rho_s W_0 F(z) \frac{d}{dz} c_i^f(z) = \Gamma(z) \left( \frac{c_i^s(z)}{D_i(z)} - c_i^f(z) \right) - \Re \left( c_i^f(z) - \frac{c_i^s(z)}{D_i(z)} \right) \quad (38)$$

$$\rho_s W_0 (1 - F(z)) \frac{d}{dz} c_i^s(z) = \Gamma(z) c_i^s(z) \left( 1 - \frac{1}{D_i(z)} \right) + \Re \left( c_i^f(z) - \frac{c_i^s(z)}{D_i(z)} \right) \quad (39)$$

182 We can now divide the fluid and solid equations by  $c_i^f$  and  $c_i^s$ , respectively, and rearrange the  $W_0$   
183 terms:

$$\frac{1}{c_i^f(z)} \frac{dc_i^f}{dz} = \frac{1}{\rho_s W_0 F(z)} \left[ \Gamma(z) \left( \frac{c_i^s(z)}{D_i(z) c_i^f(z)} - 1 \right) - \Re \left( 1 - \frac{c_i^s(z)}{D_i(z) c_i^f(z)} \right) \right] \quad (40)$$

$$\frac{1}{c_i^s(z)} \frac{dc_i^s}{dz} = \frac{1}{\rho_s W_0 (1 - F(z))} \left[ \Gamma(z) \left( 1 - \frac{1}{D_i(z)} \right) + \frac{\Re}{D_i(z)} \left( \frac{D_i(z) c_i^f(z)}{c_i^s(z)} - 1 \right) \right] \quad (41)$$

184 The first terms on the right-hand side of each of these equations are identical to pure disequilib-  
185 rium melting, such that if  $\Re$  is zero, the equations reduce to the disequilibrium transport case of  
186 Spiegelman and Elliott (1993).

187 To solve, the final terms that involve the reactivity factor can be further rewritten using the defini-  
188 tions for  $U_i^f$  and  $U_i^s$ :

$$c_i^f(z) = c_{i,0}^f \exp[U_i^f(z)] = \frac{c_{i,0}^s}{D_i^0} \exp[U_i^f(z)] \quad (42)$$

$$c_i^s(z) = c_{i,0}^s \exp[U_i^s(z)] \quad (43)$$

189 Thus:

$$\frac{D_i(z)c_i^f(z)}{c_i^s(z)} = \frac{D_i(z)}{D_i^0} \exp[U_i^f(z) - U_i^s(z)] \quad (44)$$

$$\frac{c_i^s(z)}{D_i(z)c_i^f(z)} = \frac{D_i^0}{D_i(z)} \exp[U_i^s(z) - U_i^f(z)] \quad (45)$$

190 and:

$$\frac{dU_i^f}{dz} = \frac{1}{\rho_s W_0 F(z)} \left[ \Gamma(z) \left( \frac{D_i^0}{D_i(z)} \exp[U_i^s(z) - U_i^f(z)] - 1 \right) - \Re \left( 1 - \frac{D_i^0}{D_i(z)} \exp[U_i^s(z) - U_i^f(z)] \right) \right] \quad (46)$$

$$\frac{dU_i^s}{dz} = \frac{1}{\rho_s W_0 (1 - F(z))} \left[ \Gamma(z) \left( 1 - \frac{1}{D_i(z)} \right) + \frac{\Re}{D_i(z)} \left( \frac{D_i(z)}{D_i^0} \exp[U_i^f(z) - U_i^s(z)] - 1 \right) \right] \quad (47)$$

191 Finally, substituting adiabatic upwelling and scaling with depth in place of  $\Gamma(z)$ , and adding ra-  
192 dioactive terms gives the full solutions for  $dU_i/dz$ :

$$\begin{aligned} \frac{dU_i^f}{dz} = \frac{1}{F(z)} \left[ \frac{dF}{dz} \left( \frac{D_i^0}{D_i(z)} \exp[U_i^s(z) - U_i^f(z)] - 1 \right) \right] - \frac{\Re h}{\rho_s W_0 F(z)} \left[ 1 - \frac{D_i^0}{D_i(z)} \exp[U_i^s(z) - U_i^f(z)] \right] \\ + \frac{\rho_f \phi}{\rho_s F} \lambda_i \left[ \frac{D_i^0 \alpha_{i-1}}{D_{i-1}^0 \alpha_i} \exp[U_{i-1}^f - U_i^f] - 1 \right] \end{aligned} \quad (48)$$

$$\begin{aligned} \frac{dU_i^s}{dz} = \frac{1}{(1 - F(z))} \left[ \frac{dF}{dz} \left( 1 - \frac{1}{D_i(z)} \right) \right] + \frac{\Re h}{\rho_s W_0 D_i(z) (1 - F(z))} \left[ \frac{D_i(z)}{D_i^0} \exp[U_i^f(z) - U_i^s(z)] - 1 \right] + \\ \frac{1 - \phi}{1 - F(z)} \lambda_i \left[ \frac{\alpha_{i-1}}{\alpha_i} \exp[U_{i-1}^s - U_i^s] - 1 \right] \end{aligned} \quad (49)$$

193 where  $h$  is the total height of the melting column.

194 **2.3.1 The Dahmköhler number**

195 The dimensionless combination

$$Da = \frac{\Re h}{\rho_s W_0} \quad (50)$$

196 is the Dahmköhler number, which governs the reaction rate relative to the solid transport time. If  
197 re-equilibration is limited by solid state diffusion,  $\Re$  can be estimated using:

$$\Re \approx \frac{\rho_s \mathcal{D}_i}{d^2} \quad (51)$$

198 where  $\mathcal{D}_i$  is the \*solid state\* diffusivity of element  $i$ , and  $d$  is a nominal spacing between melt-  
199 channels (this spacing could, for example, be the average grain diameter for grain-scale channels,  
200 or 10 cm for closely spaced veins).

201 In this case (which we will assume for this paper), the Dahmköhler number can be written

$$Da = \frac{D_i h}{W_0 d^2} \quad (52)$$

202 Substituting the definition of  $Da$  above yields the final dimensionless ODEs for the disequilibrium  
203 transport model:

$$\frac{dU_i^f}{dz} = \frac{1}{F(z)} \left( \frac{dF}{dz} + Da \right) \left( \frac{D_i^0}{D_i(z)} \exp[U_i^s(z) - U_i^f(z)] - 1 \right) + \frac{\rho_f \phi}{\rho_s F} \lambda_i \left[ \frac{D_i^0 \alpha_{i-1}}{D_{i-1}^0 \alpha_i} \exp[U_{i-1}^f - U_i^f] - 1 \right] \quad (53)$$

$$\frac{dU_i^s}{dz} = \frac{1}{(1-F(z))} \left[ \frac{dF}{dz} \left( 1 - \frac{1}{D_i(z)} \right) + \frac{Da}{D_i(z)} \left( \frac{D_i(z)}{D_i^0} \exp[U_i^f(z) - U_i^s(z)] - 1 \right) \right] + \frac{1-\phi}{1-F(z)} \lambda_i \left[ \frac{\alpha_{i-1}}{\alpha_i} \exp[U_{i-1}^s - U_i^s] - 1 \right] \quad (54)$$

204 with initial conditions  $U_i^s = U_i^f = 0$ .

205 In the limit where the Dahmköhler number approaches zero, the above formulas reduce to pure  
206 disequilibrium transport, whereas if  $Da$  approaches infinity (i.e., infinitely fast reactivity com-  
207 pared to physical transport), the system approaches equilibrium conditions ( $c_i^s \rightarrow D_i c_i^f$ ).

208 **2.3.2 Initial conditions**

209 Inspection of equation (53) shows that for the initial conditions described above and  $F(0) = 0$ ,  $\frac{dU_i^f}{dz}$   
210 is ill-defined (at least numerically in a floating-point system). However, taking the limit  $z \rightarrow 0$   
211 and applying L'Hôpital's rule yields

$$\lim_{z \rightarrow 0} \frac{dU_i^f}{dz} = \frac{U_i^s(0) - U_i^f(0)}{F'(0)} \left( \frac{dF}{dz} + Da \right) + \lambda_i \left[ \frac{D_i^0 \alpha_{i-1}}{D_{i-1}^0 \alpha_i} - 1 \right] \quad (55)$$

212 where

$$U_i^s(0) = \left. \frac{dU_i^s}{dz} \right|_{z=0} \quad (56)$$

$$U_i^f(0) = \left. \frac{dU_i^f}{dz} \right|_{z=0} \quad (57)$$

$$F'(0) = \left. \frac{dF}{dz} \right|_{z=0} \quad (58)$$

213 The initial radiogenic term also uses the limit from equation (34):

$$\lim_{z \rightarrow 0} \frac{\rho_f \phi}{\rho_s F} = \frac{W_0}{w(0)} = 1 \quad (59)$$

214 Rearranging equation (55) gives the value for  $U_i^f(0)$  for  $F = 0$  as

$$\lim_{z \rightarrow 0} \frac{dU_i^f}{dz} = \frac{1}{2 + \frac{Da}{F'(0)}} \left[ U_i^s(0) \left( 1 + \frac{Da}{F'(0)} \right) + \lambda_i \left[ \frac{D_i^0 \alpha_{i-1}}{D_{i-1}^0 \alpha_i} - 1 \right] \right] \quad (60)$$

## 215 3 A pyUserCalc Jupyter notebook

### 216 3.1 Code design

217 The `UserCalc` Python package implements both equilibrium and disequilibrium transport mod-  
 218 els and provides a set of code classes and utility functions for calculating and visualizing the re-  
 219 sults of one-dimensional, steady-state, partial melting forward models for both the  $^{238}\text{U}$  and  $^{235}\text{U}$   
 220 decay chains. The code package is organized into a set of Python classes and plotting routines,  
 221 which are documented in the docstrings of the classes and also demonstrated in detail below. Here  
 222 we briefly describe the overall functionality and design of the code, which is open-source and can  
 223 be modified to suit an individual researcher's needs. The code is currently available in a Git repos-  
 224 itory (<https://gitlab.com/ENKI-portal/pyUsercalc>), and any future edits or merge requests will  
 225 be managed through GitLab.

226 The equilibrium and disequilibrium transport models described above have each been imple-  
 227 mented as Python classes with a generic code interface:

```
228 ```
229 Interface:
230 -----
231 model(alpha0 , lambdas ,D,W0,F ,dFdZ , phi , rho_f=2800. , rho_s=3300. ,method=method ,Da=inf )
```

```

232
233 Parameters:
234 -----
235     alpha0 : numpy array of initial activities
236     lambdas : numpy array of decay constants scaled by solid transport time
237     D       : Function D(z) -- returns an array of partition coefficients at scaled height z
238     W0      : float -- Solid mantle upwelling rate
239     F       : Function F(z) -- returns the degree of melting F
240     dFdz    : Function dFdz(z) -- returns the derivative of F
241     phi     : Function phi(z) -- returns the porosity
242     rho_f   : float -- melt density
243     rho_s   : float -- solid density
244     method  : string -- ODE time-stepping scheme to be passed to solve_ivp (one of 'RK45', 'Radau',
245     Da      : float -- Dahmkohler Number (defaults to \inf, unused in equilibrium model)
246
247 Required Method:
248 -----
249     model.solve(): returns depth and log concentration numpy arrays z, Us, Uf
250     ...

```

251 which solves the scaled equations (i.e., equations (9) or equations (53) and (54) for the log concen-
252 trations of nuclides  $U_i^f$  and  $U_i^s$  in a decay chain of arbitrary length, with scaled decay constants  $\lambda_i'$ 
253 and initial activity ratios  $\alpha_0$ . The model equations are always solved in a one-dimensional column
254 with scaled height  $0 \leq z \leq 1$ , where bulk partition coefficients  $D_i(z)$ , degree of melting  $F(z)$ ,
255 melting rate  $dF/dz(z)$ , and porosity  $\phi(z)$  are provided by functions with height in the column.
256 Optional arguments include the melt and solid densities  $\rho_f$  and  $\rho_s$ , the Dahmköhler number  $Da$ ,
257 and the preferred numerical integration method (see `scipy.integrate.solve_ivp`).

258 `UserCalc` provides two separate model classes, `EquilTransport` and `DisequilTransport`, for
259 the different transport models; the user could add any other model that uses the same interface,
260 if desired. Most users, however, will not access the models directly but rather through the driver
261 class `UserCalc.UserCalc`, which provides support for solving and visualizing column models
262 for the relevant  $^{238}\text{U}$  and  $^{235}\text{U}$  decay chains. The general interface for the `UserCalc` class is:

```

263 ...
264 A class for constructing solutions for 1-D, steady-state, open-system U-series transport calculation
265 as in Spiegelman (2000) and Elkins and Spiegelman (submitted).
266
267 Usage:
268 -----
269
270     us = UserCalc(df,dPdz = 0.32373,n = 2.,tol=1.e-6,phi0 = 0.008,
271                 W0 =3.,model=EquilTransport, Da=None, stable=False, method='Radau')
272
273 Parameters:
274 -----
275     df : A pandas dataframe with columns ['P', 'F', 'Kr', 'DU', 'DTh', 'DRa', 'DPa']
276     dPdz : float -- Pressure gradient, to convert pressure P to depth z
277     n : float -- Permeability exponent
278     tol : float -- Tolerance for the ODE solver
279     phi0 : float -- Reference melt porosity
280     W0 : float -- Upwelling velocity (cm/yr)
281     model : class -- A U-series transport model class (one of EquilTransport or DisequilTransport)
282     Da : float -- Optional Da number for disequilibrium transport model

```

```

283     stable : bool
284         True: calculates concentrations for non-radiogenic nuclides with same chemical properties (
285         False: calculates the full radiogenic problem
286     method : string
287         ODE time-stepping method to pass to solve_ivp (usually one of 'Radau', 'BDF', or 'RK45')
288     """

```

289 The principal required input is a `pandas.DataFrame` object that provides a spreadsheet contain-  
290 ing the degree of melting  $F(P)$ , relative permeability  $K_r(P)$ , and bulk partition coefficients for  
291 the elements  $D_U$ ,  $D_{Th}$ ,  $D_{Ra}$  and  $D_{Pa}$  as functions of pressure  $P$ . The structure of the input data  
292 spreadsheet is the same as that described in Spiegelman, (2000). Once given this spreadsheet, the  
293 code routine initializes the decay constants for the isotopic decay chains and provides functions  
294 to interpolate  $F(z)$  and  $D_i(z)$  and calculate the porosity  $\phi(z)$ . Once thus initialized, the `UserCalc`  
295 class further provides the following methods:

```

296     """
297     Principal Methods:
298     -----
299     phi                : returns porosity as a function of column height
300     set_column_parameters : resets principal column parameters phi0, n, W0
301     solve_1D           : 1D column solution for a single Decay chain
302                       with arbitrary D, lambda, alpha_0
303     solve_all_1D       : Solves a single column model for both 238U and 235U chains.
304                       returns a pandas dataframe
305     solve_grid         : Solves multiple column models for a grid of porosities and upwelling
306                       returns a 3-D array of activity ratios
307     """

```

308 Of these, the principal user-facing methods are:

- 309 • `UserCalc.solve_all_1D`, which returns a `pandas.DataFrame` containing solutions for the  
310 porosity ( $\phi(z)$ ), the log concentrations of the specified nuclides in the  $^{238}\text{U}$  and  $^{235}\text{U}$  decay  
311 chains in both the melt and the solid at each interpolated depth  $z$ , and the U-series activity  
312 ratios, likewise for each depth  $z$ .
- 313 • `UserCalc.solve_grid`, which solves for a grid of one-dimensional solutions for different  
314 reference porosities ( $\phi_0$ ) and solid upwelling rates ( $W_0$ ) and returns arrays of U-series ac-  
315 tivity ratios at a specified depth (usually the top of the column), as described in Spiegelman  
316 and Elliott (1993).

### 317 3.1.1 Visualization Functions

318 In addition to the principal classes for calculating U-series activity ratios in partial melts, the  
319 `UserCalc` package also provides functions for visualizing model inputs and outputs. The pri-  
320 mary plotting functions include:

- 321 • `UserCalc.plot_inputs(df)`: Visualizes the input dataframe to show  $F(P)$ ,  $K_r(P)$  and  
322  $D_i(P)$ .
- 323 • `UserCalc.plot_1Dcolumn(df)`: Visualizes the output dataframe for a single one-  
324 dimensional melting column.

- `UserCalc.plot_contours(phi0,W0,act)` : Visualizes the output of `UserCalc.solve_grid` by generating contour plots of activity ratios at a specific depth as functions of the porosity ( $\phi_0$ ) and solid upwelling rate ( $W_0$ ).
  - `UserCalc.plot_mesh_Ra(Th,Ra,W0,phi0)` and `UserCalc.plot_mesh_Pa(Th,Pa,W0,phi0)` : Generates 'mesh' plots showing results for different  $\phi_0$  and  $W_0$  values on ( $^{226}\text{Ra}/^{230}\text{Th}$ ) vs. ( $^{230}\text{Th}/^{238}\text{U}$ ) and ( $^{231}\text{Pa}/^{235}\text{U}$ ) vs. ( $^{230}\text{Th}/^{238}\text{U}$ ) activity diagrams.
- Both the primary solver routines and visualization routines will be demonstrated in detail below.

### 3.2 An example demonstrating pyUserCalc functionality for a single melting column

The Python code cells embedded below provide an example problem that demonstrates the use and behavior of the model for a simple, two-layer upwelling mantle column, with a constant melting rate within each layer and constant  $K_r = 1$ . This example is used to compare the outcomes from the original UserCalc equilibrium model (Spiegelman, 2000) to various other implementations of the code, such as pure disequilibrium transport and scaled reactivity rates, as described above.

To use this Jupyter notebook, while in a web-enabled browser the user should select an embedded code cell by mouse-click and then simultaneously type the 'Shift' and 'Enter' keys to run the cell, after which selection will automatically advance to the following cell. The first cell below imports necessary code libraries to access the Python toolboxes and functions that will be used in the rest of the program.

```
[1]: # Select this cell with by mouseclick, and run the code by simultaneously typing
      →the 'Shift' + 'Enter' keys.
      # If the browser is able to run the Jupyter notebook, a number [1] will appear
      →to the left of the cell.

import pandas as pd
import numpy as np
import matplotlib.pyplot as plt
%matplotlib inline

# Import UserCalc:
import UserCalc
```

#### 3.2.1 Entering initial input information and viewing input data

In the full Jupyter notebook code available in the Git repository and provided here as supplementary materials, the user can edit a notebook copy and indicate their initial input data, as has been done for the sample data set below. The name for the user's input data file should be set in quotes (i.e., replacing the word 'sample' in the cell below with the appropriate filename, minus the file extension). This name will be used both to find the input file and to label any output files produced. Our sample file can likewise be downloaded and used as a formatting template for other input files (see Supplementary Materials), and is presented as a useful example below. The desired input file should be saved to a 'data' folder in the notebook directory prior to running the code.

355 Once the cell has been edited to contain the correct input file name, the user should run the cell  
356 using the technique described above.

```
[2]: runname='sample'
```

357

358 The cell below will read in the input data using the user filename specified above:

```
[3]: input_file = 'data/{}.csv'.format(runname)
df = pd.read_csv(input_file, skiprows=1, dtype=float)
df
```

359

```
[3]:
```

	P	F	Kr	DU	DTh	DRa	DPa
0	40.0	0.00000	1.0	0.00900	0.00500	0.00002	0.00001
1	39.0	0.00241	1.0	0.00900	0.00500	0.00002	0.00001
2	38.0	0.00482	1.0	0.00900	0.00500	0.00002	0.00001
3	37.0	0.00723	1.0	0.00900	0.00500	0.00002	0.00001
4	36.0	0.00964	1.0	0.00900	0.00500	0.00002	0.00001
5	35.0	0.01210	1.0	0.00900	0.00500	0.00002	0.00001
6	34.0	0.01450	1.0	0.00900	0.00500	0.00002	0.00001
7	33.0	0.01690	1.0	0.00900	0.00500	0.00002	0.00001
8	32.0	0.01930	1.0	0.00900	0.00500	0.00002	0.00001
9	31.0	0.02170	1.0	0.00900	0.00500	0.00002	0.00001
10	30.0	0.02410	1.0	0.00900	0.00500	0.00002	0.00001
11	29.0	0.02650	1.0	0.00900	0.00500	0.00002	0.00001
12	28.0	0.02890	1.0	0.00900	0.00500	0.00002	0.00001
13	27.0	0.03130	1.0	0.00900	0.00500	0.00002	0.00001
14	26.0	0.03370	1.0	0.00900	0.00500	0.00002	0.00001
15	25.0	0.03620	1.0	0.00900	0.00500	0.00002	0.00001
16	24.0	0.03860	1.0	0.00900	0.00500	0.00002	0.00001
17	23.0	0.04100	1.0	0.00899	0.00500	0.00002	0.00001
18	22.0	0.04340	1.0	0.00893	0.00498	0.00002	0.00001
19	21.0	0.04610	1.0	0.00852	0.00488	0.00002	0.00001
20	20.0	0.05000	1.0	0.00700	0.00450	0.00002	0.00001
21	19.0	0.05610	1.0	0.00548	0.00412	0.00002	0.00001
22	18.0	0.06340	1.0	0.00507	0.00402	0.00002	0.00001
23	17.0	0.07100	1.0	0.00501	0.00400	0.00002	0.00001
24	16.0	0.07860	1.0	0.00500	0.00400	0.00002	0.00001
25	15.0	0.08620	1.0	0.00500	0.00400	0.00002	0.00001
26	14.0	0.09370	1.0	0.00500	0.00400	0.00002	0.00001
27	13.0	0.10133	1.0	0.00500	0.00400	0.00002	0.00001
28	12.0	0.10892	1.0	0.00500	0.00400	0.00002	0.00001
29	11.0	0.11651	1.0	0.00500	0.00400	0.00002	0.00001
30	10.0	0.12410	1.0	0.00500	0.00400	0.00002	0.00001
31	9.0	0.13169	1.0	0.00500	0.00400	0.00002	0.00001
32	8.0	0.13928	1.0	0.00500	0.00400	0.00002	0.00001
33	7.0	0.14687	1.0	0.00500	0.00400	0.00002	0.00001
34	6.0	0.15446	1.0	0.00500	0.00400	0.00002	0.00001
35	5.0	0.16205	1.0	0.00500	0.00400	0.00002	0.00001

360

```

36  4.0  0.16964  1.0  0.00500  0.00400  0.00002  0.00001
37  3.0  0.17723  1.0  0.00500  0.00400  0.00002  0.00001
38  2.0  0.18482  1.0  0.00500  0.00400  0.00002  0.00001
39  1.0  0.19241  1.0  0.00500  0.00400  0.00002  0.00001
40  0.0  0.20000  1.0  0.00500  0.00400  0.00002  0.00001

```

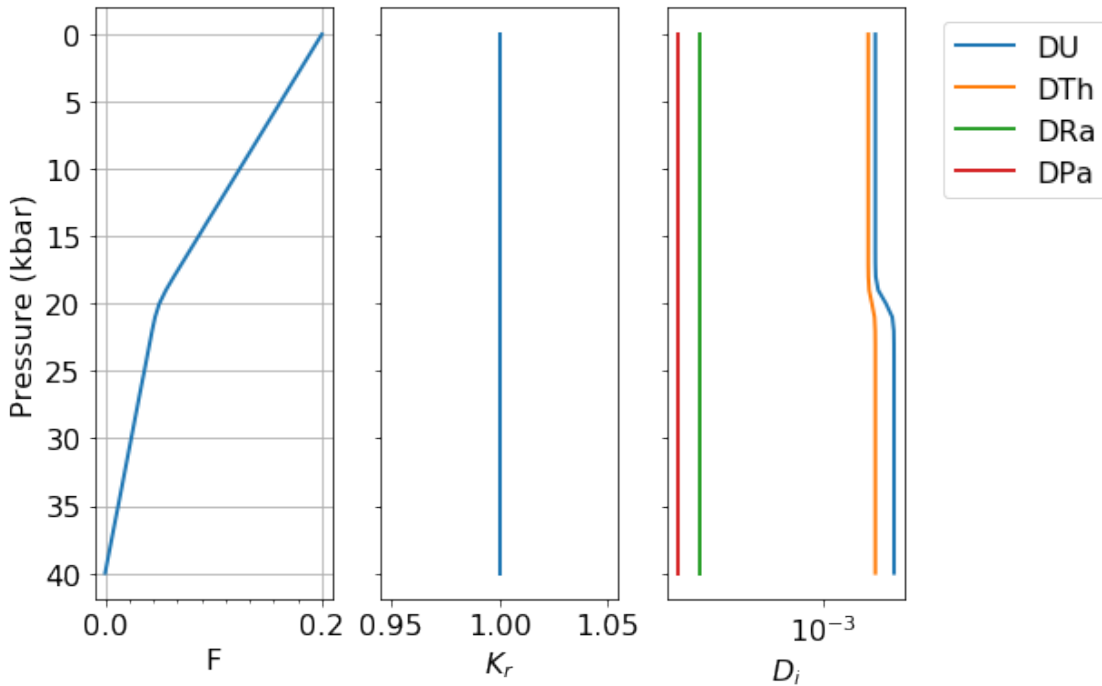
361

362 **Table 1.** Input data table for example tested here, showing pressures in kbar ( $P$ ), degree of  
363 melting ( $F$ ), permeability coefficient ( $K_r$ ), and bulk solid/melt partition coefficients ( $D_i$ ) for  
364 the elements of interest, U, Th, Ra, and Pa.

365 The next cell will visualize the input dataframe in Figure 1, using the utility function  
366 `plot_inputs`:

```
[4]: UserCalc.plot_inputs(df)
```

367



368

369 **Figure 1.** Diagrams showing example input parameters  $F$ ,  $K_r$ , and  $D_i$  as a function of pressure,  
370 for the sample input file tested here.

### 371 3.2.2 Single column equilibrium transport model

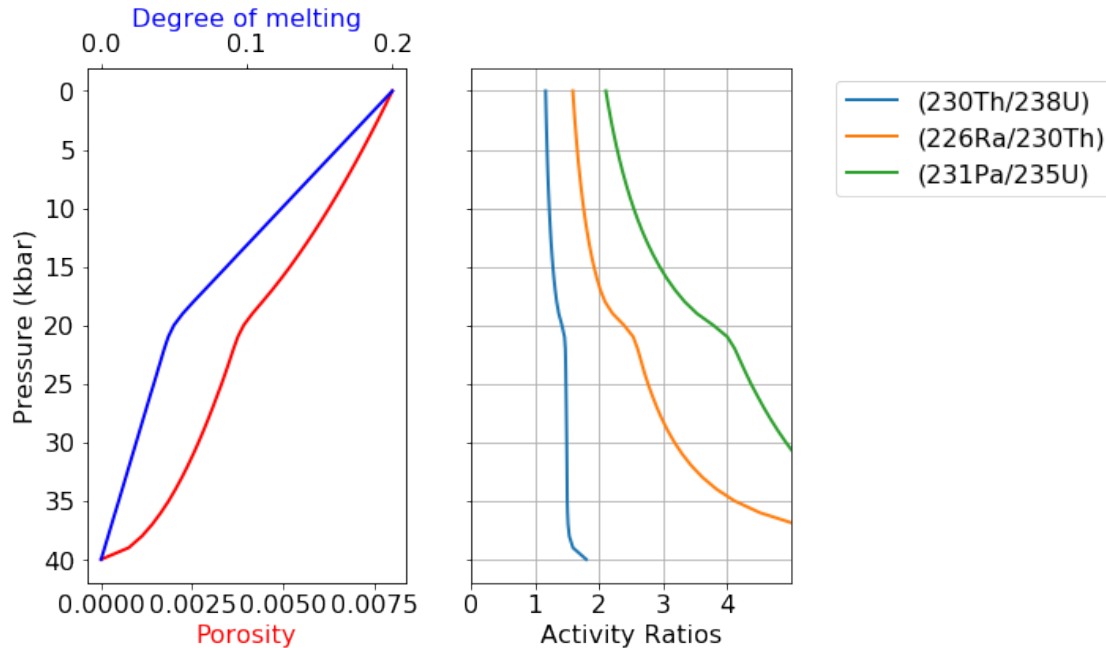
372 In its default mode, `UserCalc` solves the one-dimensional steady-state equilibrium transport  
373 model described in Spiegelman (2000). Below we will initialize the model, solve for a single col-  
374 umn and plot the results.

375 First we set the physical parameters for the upwelling column and initial conditions:

```
[5]: # Maximum melt porosity:
      phi0 = 0.008
```

376





387  
388 **Figure 2.** Equilibrium model output results for the degree of melting, residual melt porosity,  
389 and activity ratios ( $^{230}\text{Th}/^{238}\text{U}$ ), ( $^{226}\text{Ra}/^{230}\text{Th}$ ), and ( $^{231}\text{Pa}/^{235}\text{U}$ ) as a function of pressure.

### 390 3.2.3 Single column disequilibrium transport model

391 For comparison, we can repeat the calculation using the disequilibrium transport model, and  
392 compare the results to the equilibrium model. We first initialize a new model with  $Da = 0$ , which  
393 will calculate full disequilibrium transport:

```
394 [9]: us_diseq = UserCalc.UserCalc(df, model=UserCalc.DisequilTransport, Da=0.)
```

395 The cells below calculate solutions for this pure disequilibrium scenario, as shown in List 2:

```
396 [10]: df_out = us_diseq.solve_all_1D(phi0,n,W0,alpha0_all)
df_out.tail(n=1)
```

```
397 [10]:      P      z      F      phi  (230Th/238U)  (226Ra/230Th)  (231Pa/235U)  Uf_238U
40  40  0.0  0.0  0.2  0.008      1.051064      1.001054      1.055847  -3.096744

      Uf_230Th  Uf_226Ra  Us_238U  Us_230Th  Us_226Ra  Uf_235U  Uf_231Pa
40  -3.634727  -9.155135  -39.606509  -39.945908  -42.201598  -3.096769  -9.844821

      Us_235U  Us_231Pa
40  -39.602818  -45.46502
```

398 **List 2.** Model output results for the disequilibrium melting scenario tested above.

399 Next we compare the results to our equilibrium calculation above:

```
[11]: fig, axes = UserCalc.plot_1Dcolumn(df_out)
for s in ['(230Th/238U)', '(226Ra/230Th)', '(231Pa/235U)']:
    axes[2].plot(df_out_eq[s], df_out['P'], '--', color='grey')
axes[2].set_title('Da = {}'.format(us_diseq.Da))
plt.show()
```

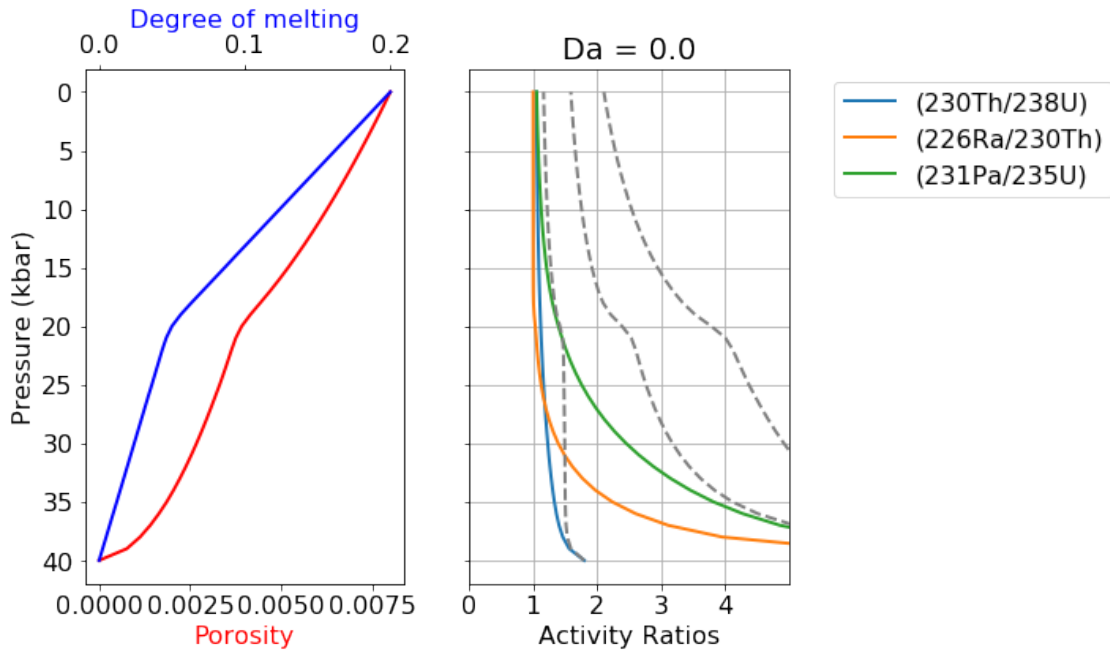


**Figure 3.** Disequilibrium model output results for the degree of melting, residual melt porosity, and activity ratios ( $^{230}\text{Th}/^{238}\text{U}$ ), ( $^{226}\text{Ra}/^{230}\text{Th}$ ), and ( $^{231}\text{Pa}/^{235}\text{U}$ ) as a function of pressure, for the Dahmköhler number shown ( $Da = 0$ ). For comparison, the dashed gray curves show solutions for the equilibrium transport model.

The dashed grey curves in Figure 3 illustrate the equilibrium transport solution, which is significantly different from the disequilibrium solution. If we increase the value of  $Da$ , however, the disequilibrium transport solution should converge towards the equilibrium scenario. To illustrate this, below we calculate the result for  $Da = 1$ :

```
[12]: us_diseq.Da=1.
df_out = us_diseq.solve_all_1D(phi0,n,W0,alpha0_all)
df_out_eq.tail(n=1)
```

```
[12]:      P      z      F      phi  (230Th/238U)  (226Ra/230Th)  (231Pa/235U)  Uf_238U
40  0.0  0.0  0.2  0.008      1.164941      1.590091      2.10557  -3.121055

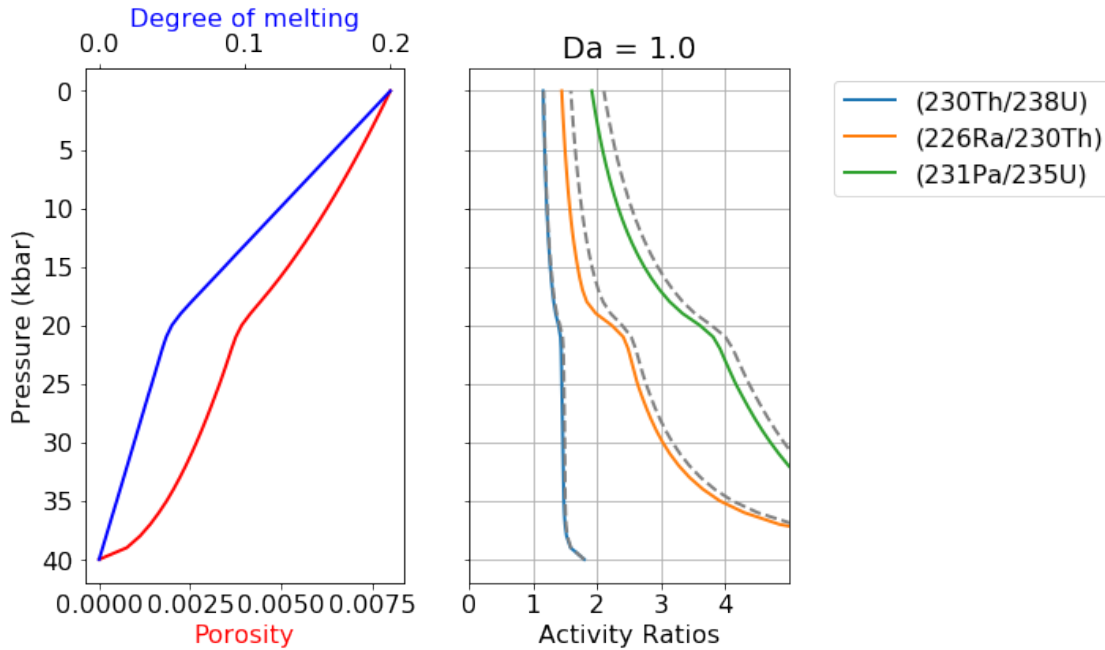
      Uf_230Th  Uf_226Ra  Us_238U  Us_230Th  Us_226Ra  Uf_235U  Uf_231Pa
40  -3.556171  -8.613841  -3.121055  -3.556171  -8.613841  -3.121909  -9.179718

      Us_235U  Us_231Pa
40  -3.121909  -9.179718
```

412 **List 3.** Model output results for the disequilibrium melting scenario tested above, where  
 413  $Da = 1$ .

```
[13]: fig, axes = UserCalc.plot_1Dcolumn(df_out)
for s in ['(230Th/238U)', '(226Ra/230Th)', '(231Pa/235U)':
    axes[2].plot(df_out_eq[s], df_out['P'], '--', color='grey')
axes[2].set_title('Da = {}'.format(us_diseq.Da))
plt.show()
```

414



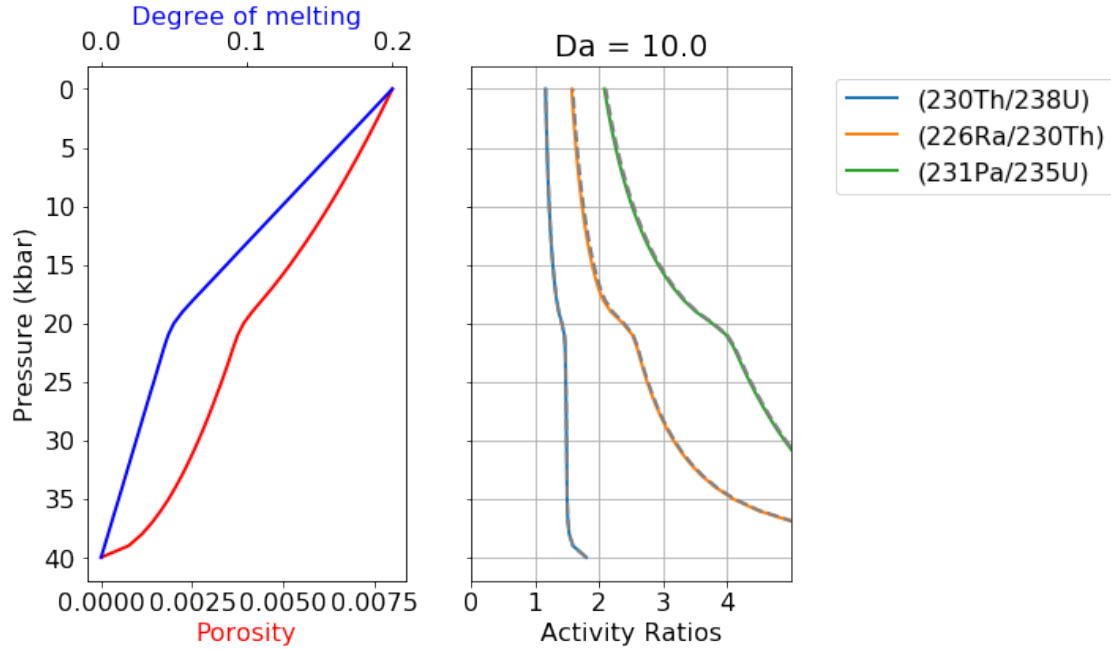
415

416 **Figure 4.** Disequilibrium model output as in Figure 3, but for  $Da = 1$ .

417 The outcome of the above calculation (Figure 4, List 3) approaches the equilibrium scenario more  
 418 closely, as predicted. Below is an additional comparison for  $Da = 10$ :

```
[14]: us_diseq.Da=10.
df_out = us_diseq.solve_all_1D(phi0,n,W0,alpha0_all)
fig, axes = UserCalc.plot_1Dcolumn(df_out)
for s in ['(230Th/238U)', '(226Ra/230Th)', '(231Pa/235U)':
    axes[2].plot(df_out_eq[s], df_out['P'], '--', color='grey')
axes[2].set_title('Da = {}'.format(us_diseq.Da))
plt.show()
```

419



420

421

**Figure 5.** Disequilibrium model output as in Figure 3, but for  $Da = 10$ .

422 For  $Da = 10$  (Figure 5), the activity ratios in the melt are indistinguishable from the equilibrium  
 423 calculation, suggesting that a Dahmköhler number of 10 is sufficiently high for a melting system  
 424 to approach chemical equilibrium, and illustrating that the equilibrium model of Spiegelman and  
 425 Elliott (1993) and Spiegelman (2000) is the limiting case for the more general disequilibrium model  
 426 presented here. For this problem, equilibrium transport always provides an upper bound on  
 427 activity ratios.

### 428 3.2.4 Stable element concentrations

429 For a stable element, i.e.,  $\lambda_i = 0$ , Spiegelman and Elliott (1993) showed that the equilibrium melt-  
 430 ing model reduces identically to simple batch melting (Shaw, 1970), while the disequilibrium  
 431 model with  $Da = 0$  is equivalent to true fractional melting. This presents a useful test of the  
 432 calculator that verifies the program is correctly calculating stable concentrations. To simulate sta-  
 433 ble element concentrations for U, Th, Ra, and Pa during equilibrium melting, we can use the same  
 434 input file example as above and simply test the scenario where  $\lambda_i$  values are equal to zero.

435 First, we impose a "stable" condition that changes all decay constants  $\lambda_i = 0$ :

```
[15]: us_eq = UserCalc.UserCalc(df, stable=True)
      df_out_eq = us_eq.solve_all_1D(phi0, n, W0, alpha0_all)
      df_out_eq.tail(n=1)
```

436

```
[15]:
```

	P	z	F	phi	(230Th/238U)	(226Ra/230Th)	(231Pa/235U)	Uf_238U
40	0.0	0.0	0.2	0.008	1.003937	1.015919	1.019959	-3.120895
	Uf_230Th	Uf_226Ra	Us_238U	Us_230Th	Us_226Ra	Uf_235U	Uf_231Pa	
40	-3.704753	-9.21042	-3.120895	-3.704753	-9.21042	-3.120895	-9.903528	

437

```

    Us_235U  Us_231Pa
40 -3.120895 -9.903528

```

438

439 **List 4.** Model output results for equilibrium porous flow melting where  $\lambda_i = 0$ , simulating  
440 stable element behavior for U, Th, Ra, and Pa and thus true (instantaneous) batch melting.

441 For comparison with the results in List 4, we can use the batch melting equation (Shaw, 1970) to  
442 calculate the concentrations of U, Th, Ra, and Pa using the input values in Table 1 for  $F(z)$  and  $D_i$ ,  
443 where:

$$\frac{c_i^f}{c_i^0} = \frac{1}{F + D_i(1 - F)} \quad (61)$$

444 and determine radionuclide activities for the batch melt using the definition of the activity  $a$  for a  
445 nuclide  $i$ :

$$a_i = \lambda_i c_i^f \quad (62)$$

446 and the initial nuclide activities  $a_i^0$ , such that:

$$a_i = \frac{a_i^0}{F + D_i(1 - F)} \quad (63)$$

447 As the activity ratios in List 5 illustrate, the outcomes of this simple batch melting equation are  
448 identical to those produced by the model for equilibrium transport and  $\lambda = 0$ .

```

[16]: df_batch=df[['P', 'F', 'DU', 'DTh', 'DRa', 'DPa']]
df_batch['(230Th/238U)'] = (alpha0_all[1]/(df_batch.F-df_batch.F*df_batch.
    ↳DTh+df_batch.DTh))/(alpha0_all[0]/(df_batch.F-df_batch.F*df_batch.DU+df_batch.
    ↳DU))
df_batch['(226Ra/230Th)'] = (alpha0_all[2]/(df_batch.F-df_batch.F*df_batch.
    ↳DRa+df_batch.DRa))/(alpha0_all[1]/(df_batch.F-df_batch.F*df_batch.DTh+df_batch.
    ↳DTh))
df_batch['(231Pa/235U)'] = (alpha0_all[4]/(df_batch.F-df_batch.F*df_batch.
    ↳DPa+df_batch.DPa))/(alpha0_all[3]/(df_batch.F-df_batch.F*df_batch.DU+df_batch.
    ↳DU))

# Extract columns and concatenate dataframes
cols = ['P', 'F', '(230Th/238U)', '(226Ra/230Th)', '(231Pa/235U)']
df_compare = pd.concat([ df_batch[cols].tail(1), df_out_eq[cols].tail(1)])
df_compare['model'] = ['Batch Melting', 'Equilibrium Transport: stable elements']
df_compare.set_index('model')

```

449

```

[16]:          P      F  (230Th/238U)  (226Ra/230Th)
model

```

450

```

Batch Melting                0.0  0.2    1.003937    1.015919
Equilibrium Transport: stable elements 0.0  0.2    1.003937    1.015919

```

(231Pa/235U)

```

model
Batch Melting                1.019959
Equilibrium Transport: stable elements 1.019959

```

451

452 **List 5.** Simple batch melting calculation results using the methods of Shaw (1970), demon-  
453 strating identical activity ratio results to those calculated using the equilibrium transport  
454 model with  $\lambda_i = 0$ .

455 Similarly, we can also determine pure disequilibrium melting using the disequilibrium transport  
456 model with  $\lambda_i = 0$ . A simple fractional melting problem is easiest to test using constant melt pro-  
457 ductivity and partitioning behavior, so here we test a simplified, one-layer scenario with constant  
458  $dF/dz$  and  $D_i$  values:

```

[17]: input_file_2 = 'data/simple_sample.csv'
      df_test = pd.read_csv(input_file_2, skiprows=1, dtype=float)
      UserCalc.plot_inputs(df_test)
      df_test.tail(n=1)

```

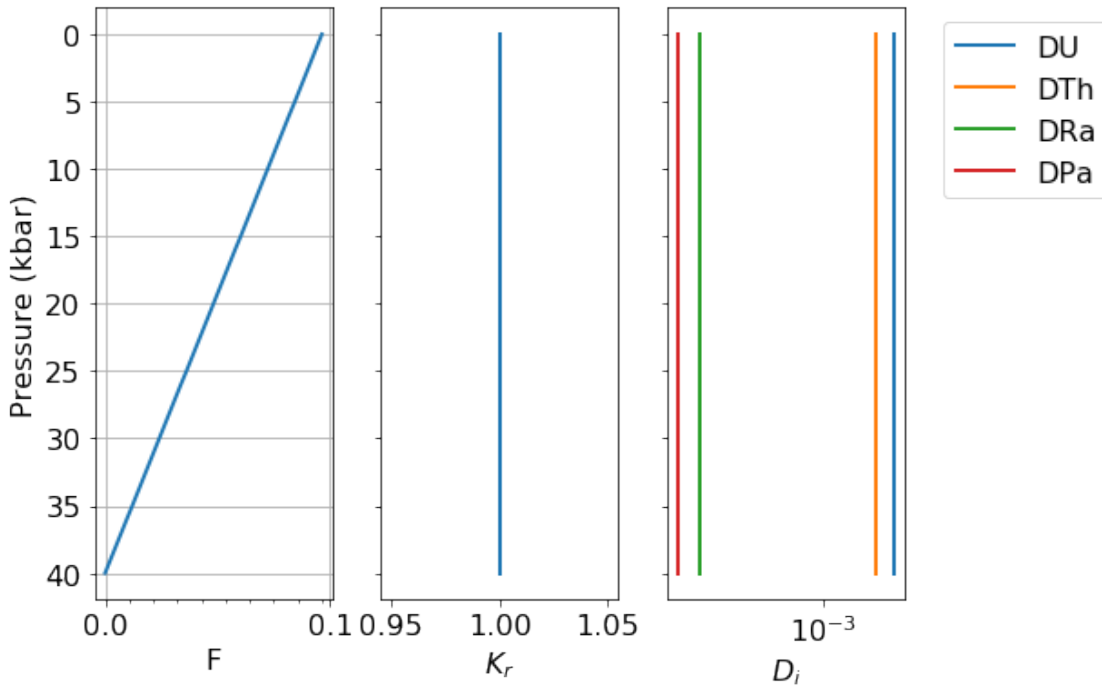
459

```

[17]:      P      F  Kr   DU  DTh   DRa   DPa
460 40  0.0  0.0964  1.0  0.009  0.005  0.00002  0.00001

```

460



461

462 **Figure 6.** Simple alternative input file with constant melt productivity and constant  
463 solid/melt partitioning, used here to test pure fractional melting outputs.

464 We note that numerical ODE solvers may not successfully solve for pure fractional melting with  
 465  $Da = 0$  and stable elements, because the resulting extreme changes in solid concentrations for  
 466 highly incompatible elements are difficult to resolve using numerical methods. Stable solutions  
 467 can nonetheless be obtained for very small values of  $Da$  that approach  $Da = 0$ , and such solutions  
 468 still provide a useful test of the disequilibrium transport model. Here we use  $Da = 10^{-10}$ ; for such  
 469 low  $Da$  values, the liquid closely approaches the composition of an accumulated fractional melt,  
 470 and although the liquid and solid outcomes are slightly different from pure fractional melting, the  
 471 solid is still essentially depleted of all incompatible nuclides.

```
[18]: us_diseq_test = UserCalc.UserCalc(df_test, model=UserCalc.  
      ↪DisequilTransport, stable=True, Da=1.e-10)
```

```
[19]: df_diseq_test = us_diseq_test.solve_all_1D(phi0,n,W0,alpha0_all)
```

474 Similar to our approach for equilibrium and batch melting, we can compare the results of dise-  
 475 quilibrium transport for stable elements with pure fractional melting for constant partition coeffi-  
 476 cients using the definition of aggregated fractional melt concentrations (Figure 7):

$$\frac{c_i^s}{c_i^{s,0}} = (1 - F)^{1/D_i - 1} \quad (64)$$

$$\frac{c_i^f}{c_i^{f,0}} = \frac{D_i}{F} \left( 1 - (1 - F)^{1/D_i} \right) \quad (65)$$

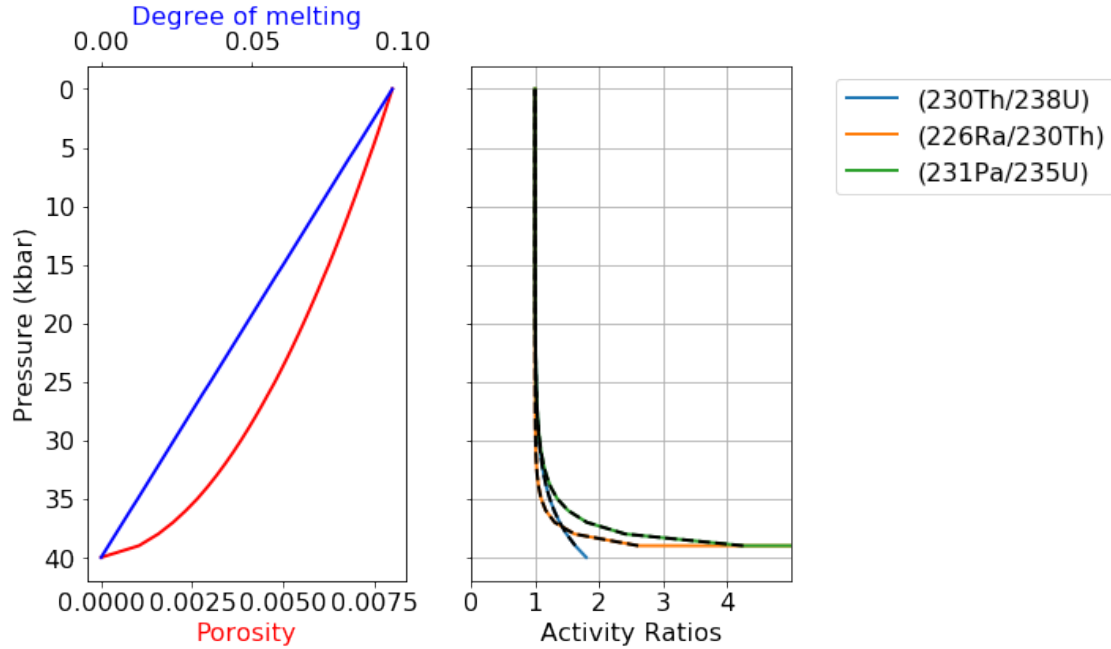
477 or in log units:

$$U_i^s = (1/D_i - 1) \log(1 - F) \quad (66)$$

$$U_i^f = \log \left( 1 - (1 - F)^{1/D_i} \right) + \log \left( \frac{D_i}{F} \right) \quad (67)$$

```
[20]: df_frac=df_test[['P', 'F', 'DU', 'DTh', 'DRa', 'DPa']]  
df_frac['(230Th/238U)'] = ((alpha0_all[1]/df_frac.F)*(1.-(1.-df_frac.F)**(1./  
      ↪df_frac.DTh))) / ((alpha0_all[0]/df_frac.F)*(1.-(1.-df_frac.F)**(1./df_frac.  
      ↪DU)))  
df_frac['(226Ra/230Th)'] = ((alpha0_all[2]/df_frac.F)*(1.-(1.-df_frac.F)**(1./  
      ↪df_frac.DRa))) / ((alpha0_all[1]/df_frac.F)*(1.-(1.-df_frac.F)**(1./df_frac.  
      ↪DTh)))  
df_frac['(231Pa/235U)'] = ((alpha0_all[4]/df_frac.F)*(1.-(1.-df_frac.F)**(1./  
      ↪df_frac.DPa))) / ((alpha0_all[3]/df_frac.F)*(1.-(1.-df_frac.F)**(1./df_frac.  
      ↪DU)))
```

```
[21]: fig, axes = UserCalc.plot_1Dcolumn(df_diseq_test)  
for s in ['(230Th/238U)', '(226Ra/230Th)', '(231Pa/235U)']:  
    axes[2].plot(df_frac[s], df_diseq_test['P'], '--', color='black')  
plt.show()
```



480

481

482

483

484

485

**Figure 7.** Model output results for the degree of melting, residual melt porosity, and activity ratios ( $^{230}\text{Th}/^{238}\text{U}$ ), ( $^{226}\text{Ra}/^{230}\text{Th}$ ), and ( $^{231}\text{Pa}/^{235}\text{U}$ ) as a function of pressure. The solid curves plot the results of pure fractional melting for stable elements, while the dashed black curves illustrate the outcomes of the disequilibrium transport model with  $Da = 10^{-10}$  and  $\lambda_i = 0$ . The outcomes of the two methods are indistinguishable.

### 486 3.2.5 Considering lithospheric transport scenarios

487 In mantle decompression melting scenarios, melting is expected to cease in the shallow, colder  
 488 part of the regime where a lithospheric layer is present. The effects of cessation of melting prior  
 489 to reaching the surface can be envisioned as affecting magma compositions in a number of ways,  
 490 some of which could be calculated using the models presented here by setting  $dF = 0$ .

491 There are, however, several limitations when using our transport models to simulate lithospheric  
 492 melt transport in this way, as the model equations are written to track steady-state decompression  
 493 and melting. The first limitation is thus the underlying assumption that the solid is migrating and  
 494 experiencing progressive melt depletion in the model, while the solid lithosphere should in fact  
 495 behave as a rigid matrix that does not experiencing upwelling. For the disequilibrium transport  
 496 model with  $Da = 0$ , no chemical reequilibration occurs while  $dF = 0$ , so the lack of solid migration  
 497 after the cessation of melting does not pose a problem; instead, in the pure disequilibrium trans-  
 498 port case, imposing  $dF = 0$  simply allows for radioactive decay and ingrowth during transport  
 499 through the lithospheric layer.

500 The equilibrium transport model, on the other hand, permits full equilibration even if  $dF = 0$ ,  
 501 but the liquid composition does not directly depend on the solid concentration,  $c_i^s(z)$ , so ongoing  
 502 chemical reequilibration between the liquid and a modified lithospheric solid could be simulated  
 503 by modifying the bulk solid/liquid partition coefficients  $D_i$ . However, the underlying model  
 504 assumes that the liquid with mass proportion  $F_{max}$  reequilibrates with the solid matrix in a steady-  
 505 state transport regime, at the maximum reference porosity, which may not accurately simulate the

506 transport regime through the fixed lithosphere with no melting.

507 The case of the scaled disequilibrium transport model with  $Da > 0$  is the most complex, since the  
508 model directly calculates reequilibration of the liquid with a progressively melting solid layer, and  
509 thus may not accurately simulate transport through the fixed solid lithosphere. We advise that if  
510 the model is used in this way, the results must be interpreted with caution.

511 Finally, calculating a given transport model through the upwelling asthenosphere and into a fixed  
512 overlying lithospheric layer neglects an additional, significant limitation: namely that melt-rock  
513 interactions, and thus the magma transport style, may be different in the lithosphere than in the  
514 melting asthenosphere. While it is not possible to change transport models during a single 1D run  
515 in the current implementation, one alternative approach is to change the relative permeability,  $K_r$ ,  
516 in the lithosphere, in addition to modifying the bulk partition coefficients to reflect lithospheric  
517 values. It may also be possible to run a separate, second-stage lithospheric calculation with mod-  
518 ified input parameters and revised liquid porosity constraints, but this option is not currently  
519 implemented and would require an expansion of the current model.

520 Despite these caveats, there are some limited scenarios where users may wish to simulate equilib-  
521 rium or disequilibrium magma transport through a capping layer with constant  $dF = 0$ , constant  
522  $\phi = \phi_0$ , and revised  $D_i$  values for a modified layer mineralogy. The cells below provide options  
523 for modifying the existing input data table to impose such a layer. The first cell identifies a final  
524 melting pressure  $P_{Lithos}$ , which is defined by the user in kbar. This value can be set to 0.0 if no  
525 lithospheric cap is desired; in the example below, it has been set at 5.0 kbar. There are two over-  
526 all options for how this final melting pressure could be used to modify the input data. The first  
527 option (implemented in the Supplementary Materials but not tested here) simply deletes all lines  
528 in the input dataframe for depths shallower than  $P_{Lithos}$ . This is a straightforward option for a  
529 one-dimensional column scenario, where melting simply stops at the base of the lithosphere and  
530 the composition of the melt product is observed in that position. This is an effective way to limit  
531 further chemical interactions after melting has ceased; it fails to account for additional radioactive  
532 decay during lithospheric melt transport, but subsequent isotopic decay over a fixed transport  
533 time interval could then be calculated using the radioactive decay equations for U-series nuclides.

534 A second option, shown here to demonstrate outcomes, changes the degree of melting increments  
535 ( $dF$ ) to a value of 0 for all depths shallower than  $P_{Lithos}$ , but allows model calculations to con-  
536 tinue at shallower depths. This is preferable if the user aims to track additional radioactive decay  
537 and/or chemical exchange after melting has ceased and during subsequent transport through the  
538 lithospheric layer, and shall be explored further below.

```
[22]: Plithos = 5.0

Pfinal = df.iloc[(df['P']-Plithos).abs().idxmin()]
F_max = Pfinal[1].tolist()
df.loc[(df['P'] < Plithos),['F']] = F_max
```

540 For equilibrium transport scenarios, the cell below offers one possible option for modifying litho-  
541 spheric solid/melt bulk partition coefficients. We note that if the disequilibrium transport model  
542 is used with  $Da = 0$  (i.e., pure chemical disequilibrium), this cell is not necessary.

543 The option demonstrated below imposes new, constant melt-rock partition coefficients during  
544 lithospheric transport. These values are assumed to be fixed. An alternative choice, included in

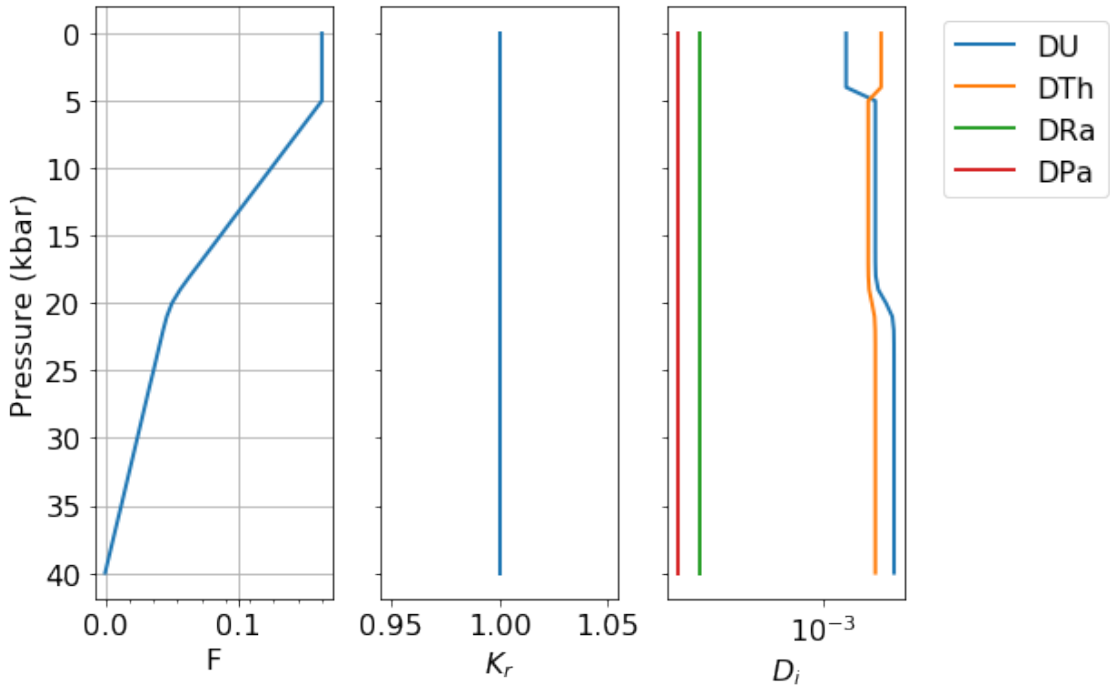
545 the Supplementary Materials, instead fixes the shallower lithospheric solid/melt bulk partition  
 546 coefficients such that they are equal to  $D_i$  values at the depth where melting ceased (i.e.,  $P_{Lithos}$ ).

```
[23] : # Define new bulk solid/liiquid partition coefficients for the lithospheric
      → layer:
      D_U_lith = 0.002
      D_Th_lith = 0.006
      D_Ra_lith = 0.00002
      D_Pa_lith = 0.00001

      # Implement the changed values defined above:
      df.loc[(df['P'] < Plithos),['DU']] = D_U_lith
      df.loc[(df['P'] < Plithos),['DTh']] = D_Th_lith
      df.loc[(df['P'] < Plithos),['DRa']] = D_Ra_lith
      df.loc[(df['P'] < Plithos),['DPa']] = D_Pa_lith
```

548 Following any changes implemented above, the cells below will process and display the refined  
 549 input data (Figure 8, Table 2).

```
[24] : UserCalc.plot_inputs(df)
```



551  
 552 **Figure 8.** Diagrams showing input parameters  $F$ ,  $K_r$ , and  $D_i$  as a function of pressure, for the  
 553 example input file and modified lithospheric conditions.

```
[25] : df
```

[25] :

	P	F	Kr	DU	DTh	DRa	DPa
0	40.0	0.00000	1.0	0.00900	0.00500	0.00002	0.00001
1	39.0	0.00241	1.0	0.00900	0.00500	0.00002	0.00001
2	38.0	0.00482	1.0	0.00900	0.00500	0.00002	0.00001
3	37.0	0.00723	1.0	0.00900	0.00500	0.00002	0.00001
4	36.0	0.00964	1.0	0.00900	0.00500	0.00002	0.00001
5	35.0	0.01210	1.0	0.00900	0.00500	0.00002	0.00001
6	34.0	0.01450	1.0	0.00900	0.00500	0.00002	0.00001
7	33.0	0.01690	1.0	0.00900	0.00500	0.00002	0.00001
8	32.0	0.01930	1.0	0.00900	0.00500	0.00002	0.00001
9	31.0	0.02170	1.0	0.00900	0.00500	0.00002	0.00001
10	30.0	0.02410	1.0	0.00900	0.00500	0.00002	0.00001
11	29.0	0.02650	1.0	0.00900	0.00500	0.00002	0.00001
12	28.0	0.02890	1.0	0.00900	0.00500	0.00002	0.00001
13	27.0	0.03130	1.0	0.00900	0.00500	0.00002	0.00001
14	26.0	0.03370	1.0	0.00900	0.00500	0.00002	0.00001
15	25.0	0.03620	1.0	0.00900	0.00500	0.00002	0.00001
16	24.0	0.03860	1.0	0.00900	0.00500	0.00002	0.00001
17	23.0	0.04100	1.0	0.00899	0.00500	0.00002	0.00001
18	22.0	0.04340	1.0	0.00893	0.00498	0.00002	0.00001
19	21.0	0.04610	1.0	0.00852	0.00488	0.00002	0.00001
20	20.0	0.05000	1.0	0.00700	0.00450	0.00002	0.00001
21	19.0	0.05610	1.0	0.00548	0.00412	0.00002	0.00001
22	18.0	0.06340	1.0	0.00507	0.00402	0.00002	0.00001
23	17.0	0.07100	1.0	0.00501	0.00400	0.00002	0.00001
24	16.0	0.07860	1.0	0.00500	0.00400	0.00002	0.00001
25	15.0	0.08620	1.0	0.00500	0.00400	0.00002	0.00001
26	14.0	0.09370	1.0	0.00500	0.00400	0.00002	0.00001
27	13.0	0.10133	1.0	0.00500	0.00400	0.00002	0.00001
28	12.0	0.10892	1.0	0.00500	0.00400	0.00002	0.00001
29	11.0	0.11651	1.0	0.00500	0.00400	0.00002	0.00001
30	10.0	0.12410	1.0	0.00500	0.00400	0.00002	0.00001
31	9.0	0.13169	1.0	0.00500	0.00400	0.00002	0.00001
32	8.0	0.13928	1.0	0.00500	0.00400	0.00002	0.00001
33	7.0	0.14687	1.0	0.00500	0.00400	0.00002	0.00001
34	6.0	0.15446	1.0	0.00500	0.00400	0.00002	0.00001
35	5.0	0.16205	1.0	0.00500	0.00400	0.00002	0.00001
36	4.0	0.16205	1.0	0.00200	0.00600	0.00002	0.00001
37	3.0	0.16205	1.0	0.00200	0.00600	0.00002	0.00001
38	2.0	0.16205	1.0	0.00200	0.00600	0.00002	0.00001
39	1.0	0.16205	1.0	0.00200	0.00600	0.00002	0.00001
40	0.0	0.16205	1.0	0.00200	0.00600	0.00002	0.00001

555

556

557

558

**Table 2.** Input data table for an example scenario with modified lithospheric transport conditions, showing pressures in kbar ( $P$ ), degree of melting ( $F$ ), permeability coefficient ( $K_r$ ), and bulk solid/melt partition coefficients ( $D_i$ ) for the elements of interest, U, Th, Ra, and Pa.

559 The cells below will rerun the end member models for the modified lithospheric input file. First,  
 560 equilibrium transport:

```
[26]: us_eq = UserCalc.UserCalc(df,stable=False)
      df_out_eq = us_eq.solve_all_1D(phi0,n,W0,alpha0_all)
```

562 And second, for disequilibrium transport with  $Da = 0$ :

```
[27]: us_diseq = UserCalc.UserCalc(df,model=UserCalc.
      →DisequilTransport, Da=0, stable=False)
      df_out_diseq = us_diseq.solve_all_1D(phi0,n,W0,alpha0_all)
```

564 List 6 below displays the activity ratios determined for the final melt compositions at the end of  
 565 the two simulations (i.e., the tops of the one-dimensional melting columns).

```
[28]: df_compare = pd.concat([df_out_eq.tail(n=1), df_out_diseq.tail(n=1)])
      df_compare['model'] = ['Equilibrium Transport', 'Disequilibrium Transport']
      df_compare.set_index('model')
```

```
[28]:
```

	P	z	F	phi	(230Th/238U)
model					
Equilibrium Transport	0.0	0.0	0.16205	0.008	1.015792
Disequilibrium Transport	0.0	0.0	0.16205	0.008	1.039704

	(226Ra/230Th)	(231Pa/235U)	Uf_238U	Uf_230Th
model				
Equilibrium Transport	1.894057	1.792975	-2.901132	-3.473250
Disequilibrium Transport	1.000828	1.034719	-2.891833	-3.440684

	Uf_226Ra	Us_238U	Us_230Th	Us_226Ra	Uf_235U
model					
Equilibrium Transport	-8.355990	-2.901132	-3.473250	-8.355990	-2.902001
Disequilibrium Transport	-8.961317	-30.351986	-30.353121	-30.353146	-2.884920

	Uf_231Pa	Us_235U	Us_231Pa
model			
Equilibrium Transport	-9.120520	-2.902001	-9.120520
Disequilibrium Transport	-9.653185	-30.272812	-30.272749

568 **List 6.** Model output results for the disequilibrium ( $Da = 0$ ) melting scenarios tested here,  
 569 with modified lithospheric input conditions.

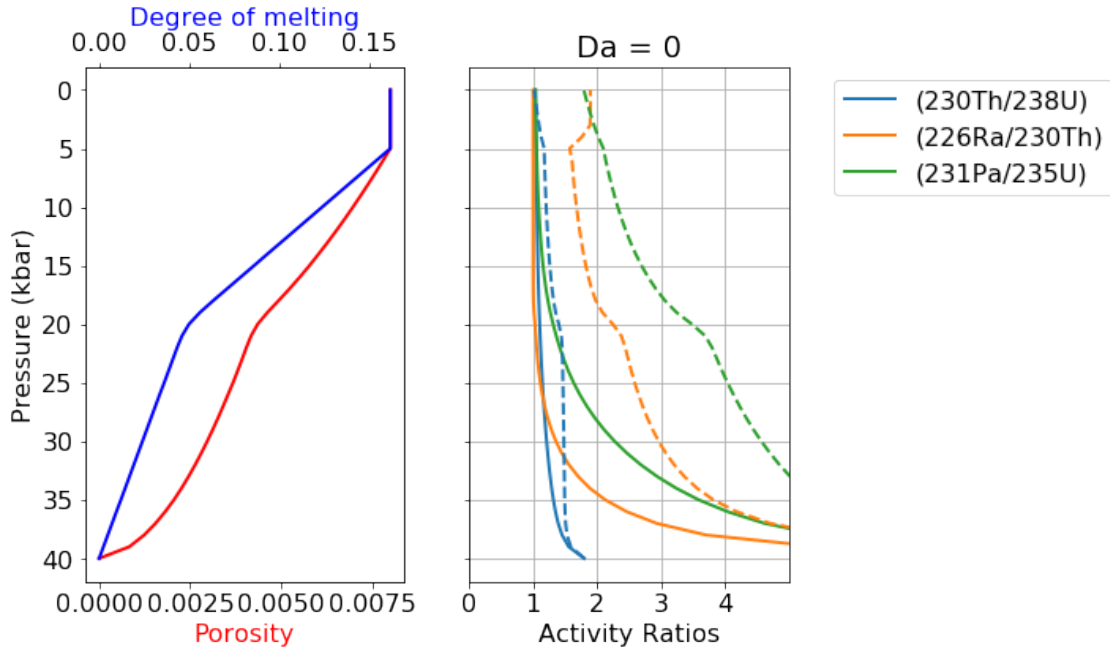
570 The following cell generates Figure 9, which illustrates outcomes with depth for the equilibrium  
 571 and disequilibrium transport models. The model outcomes for the two transport scenarios are  
 572 notably different, particularly for the shorter-lived isotopic pairs.

```

[29]: fig, axes = UserCalc.plot_1Dcolumn(df_out_diseq)
      axes[2].set_prop_cycle(None)
      for s in ['(230Th/238U)', '(226Ra/230Th)', '(231Pa/235U)':
          axes[2].plot(df_out_eq[s], df_out['P'], '--')
      axes[2].set_title('Da = {}'.format(us_diseq.Da))
      plt.show()

```

573



574

575

576

577

578

**Figure 9.** Comparison of equilibrium (dashed) and disequilibrium ( $Da = 0$ ; solid) transport model output results for the degree of melting, residual melt porosity, and activity ratios ( $^{230}\text{Th}/^{238}\text{U}$ ), ( $^{226}\text{Ra}/^{230}\text{Th}$ ), and ( $^{231}\text{Pa}/^{235}\text{U}$ ) as a function of pressure, for the modified lithospheric transport scenario explored above. Symbols and lines as in Figure 3.

579

### 3.3 Batch operations

580

581

582

583

584

585

586

587

588

589

590

591

For many applications, it is preferable to run a batch of model scenarios over a range of input parameters directly related to questions about the physical constraints on melt generation, such as the maximum residual or reference melt porosity ( $\phi_0$ ) and the solid mantle upwelling rate ( $W_0$ ). The cells below determine a series of one-dimensional column results for the desired transport model for the parameters defined above, but over a range of values for  $\phi_0$  and  $W_0$ ; these results are then shown in a series of figures and exported as data tables. The user can select whether to define the specific  $\phi_0$  and  $W_0$  values as evenly spaced log grid intervals (option 1) or with manually specified values (option 2). As above, all upwelling rates are entered in units of cm/yr. We note that because some of these models tend to be stiff and the Radau solver is relatively expensive, the batch operations below may require a few minutes of computation time for certain scenarios. Here we show the results for the default equilibrium model over a range of selected  $\phi_0$  and  $W_0$  values of interest:

```

[30]: # Option 1 (evenly spaced log grid intervals):
# phi0 = np.logspace(-3,-2,11)
# W0 = np.logspace(-1,1,11)

# Option 2 (manual selection of values):
phi0 = np.array([0.001, 0.002, 0.005, 0.01])
W0 = np.array([0.5, 1., 2., 5., 10., 20., 50.])

import time
tic = time.perf_counter()
toc = time.perf_counter()

# Calculate the U-238 decay chain grid values:
act = us_eq.solve_grid(phi0, n, W0, us_eq.D_238, us_eq.lambdas_238, us_eq.
    ↪alphas_238)
Th = act[0]
Ra = act[1]
df = pd.DataFrame(Th)
df = pd.DataFrame(Ra)

```

592

```

W = 0.5 . . . .
W = 1.0 . . . .
W = 2.0 . . . .
W = 5.0 . . . .
W = 10.0 . . . .
W = 20.0 . . . .
W = 50.0 . . . .

```

```

[31]: # Calculate the U-235 decay chain grid values:
act_235 = us_eq.solve_grid(phi0, n, W0, us_eq.D_235, us_eq.lambdas_235, us_eq.
    ↪alphas_235)
Pa = act_235[0]
df = pd.DataFrame(Pa)

```

593

```

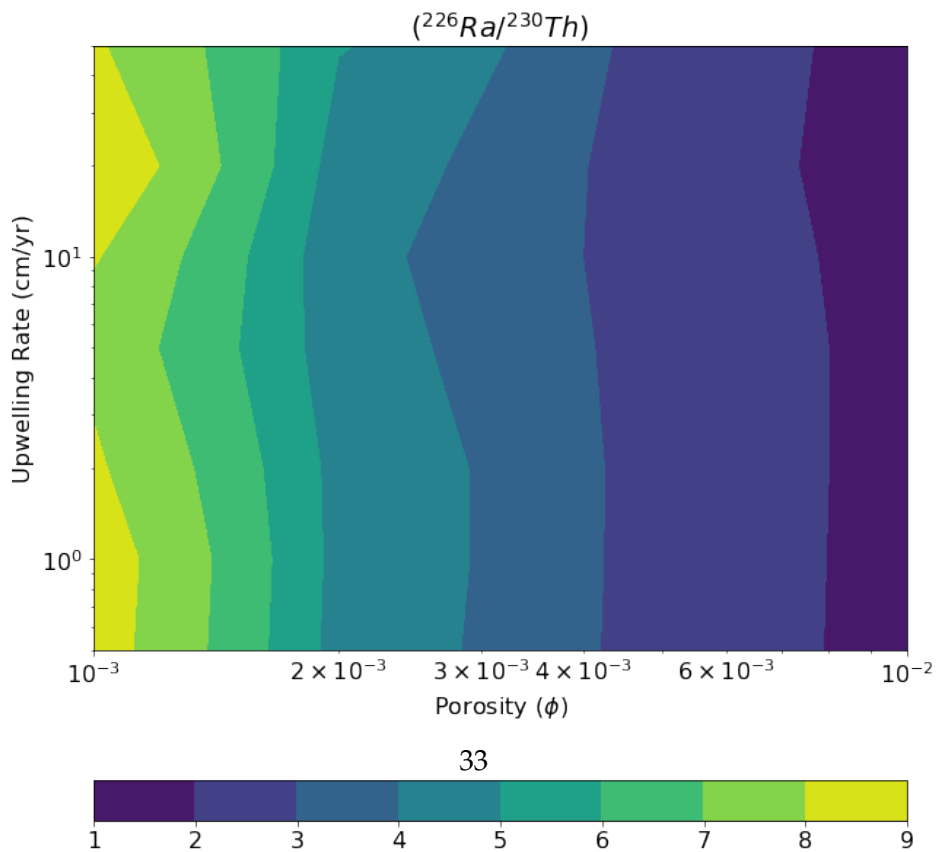
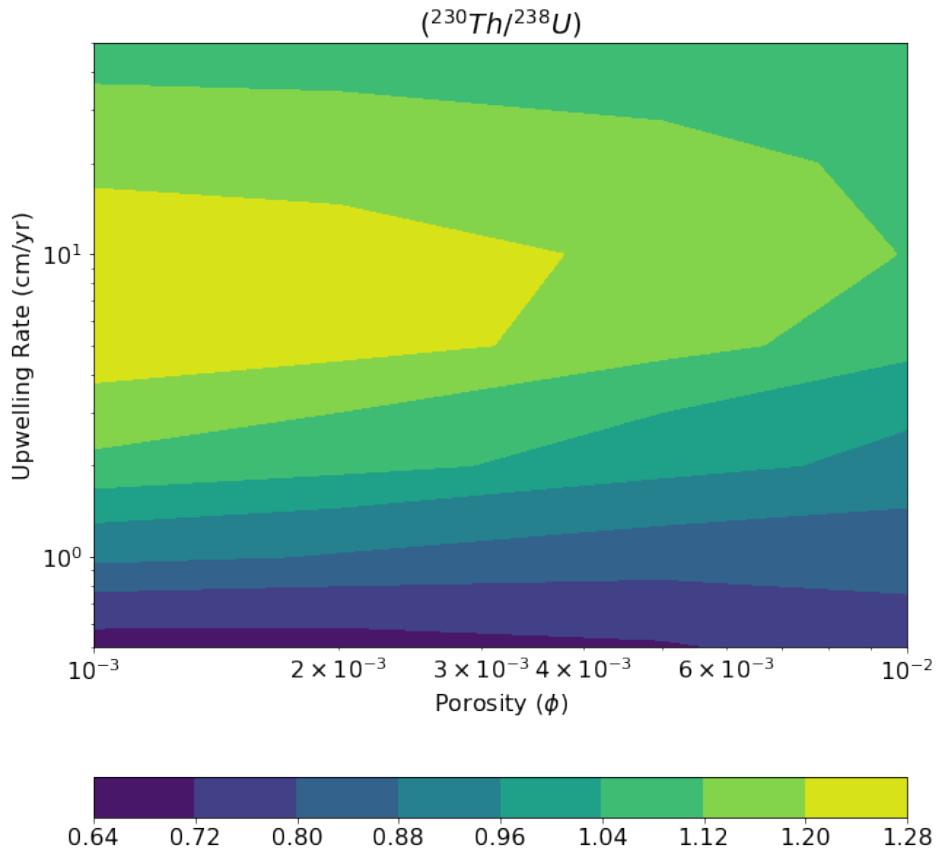
W = 0.5 . . . .
W = 1.0 . . . .
W = 2.0 . . . .
W = 5.0 . . . .
W = 10.0 . . . .
W = 20.0 . . . .
W = 50.0 . . . .

```

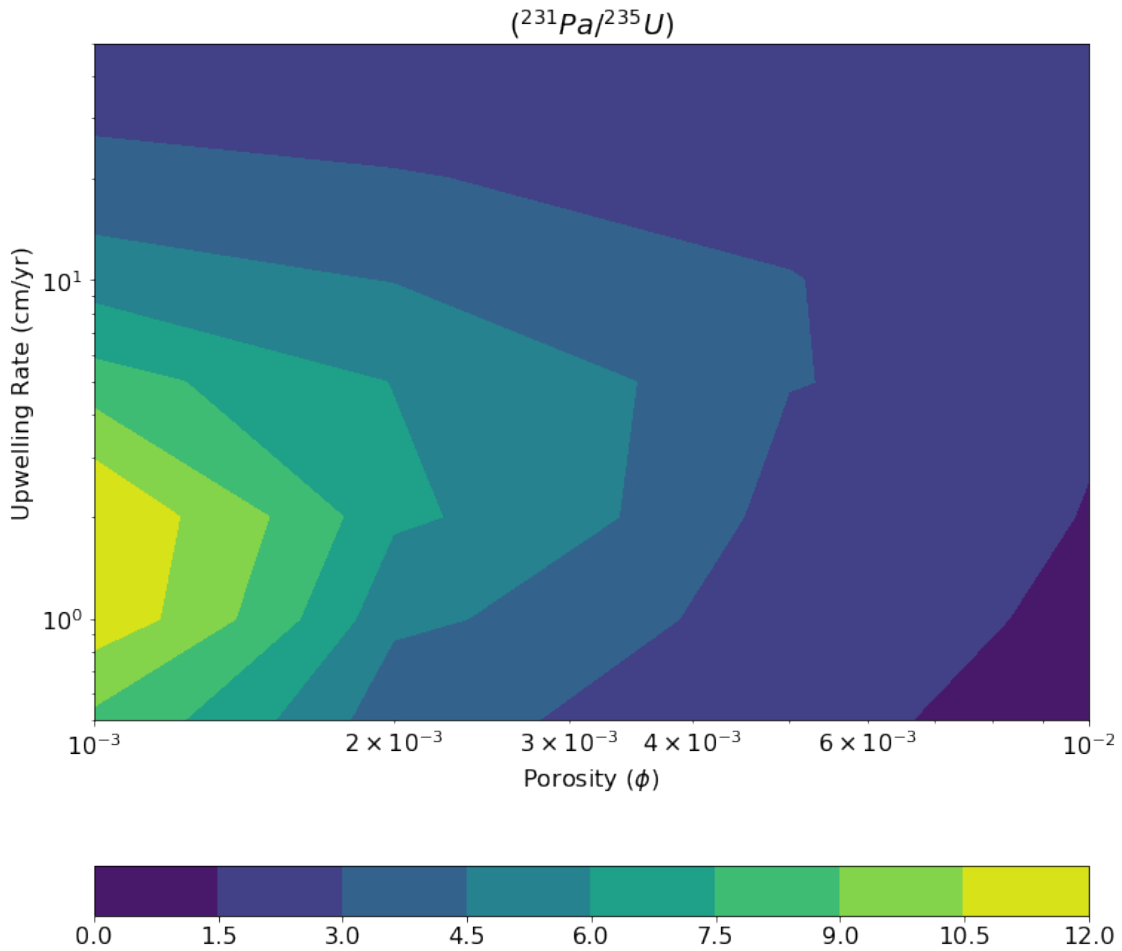
594 The figures below illustrate the batch model results in a variety of ways. First, each isotopic  
595 activity ratio is contoured in  $\phi_0$  vs.  $W_0$  space (Figure 10), and then outcomes for  $W_0$  and  $\phi_0$  values  
596 are contoured as mesh "grids" in activity ratio-activity ratio plots (Figure 11).

```
[32]: UserCalc.plot_contours(phi0,W0,act, figsize=(12,12))
```

597



[33] : UserCalc.plot\_contours(phi0,W0,act\_235)  
599



600

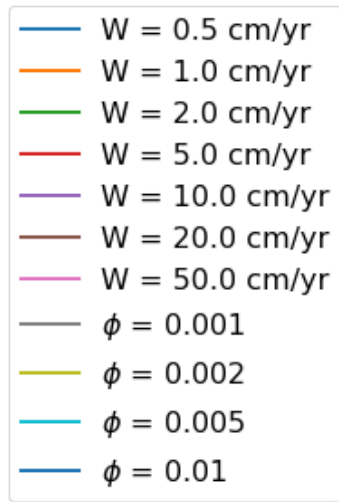
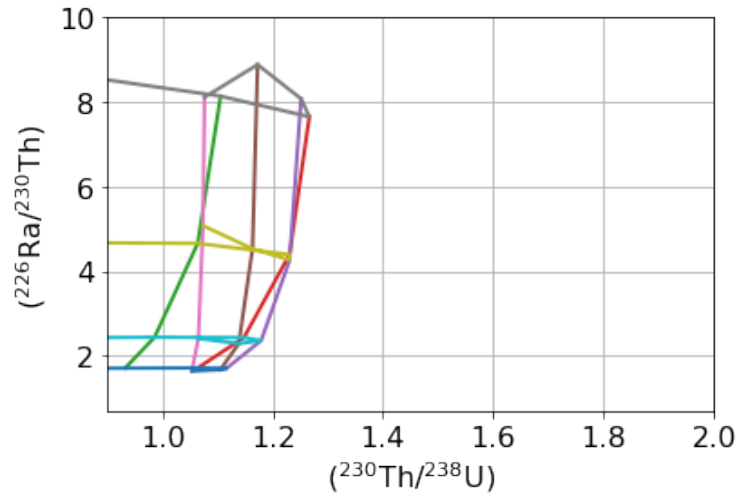
601

602

603

**Figure 10.** Diagrams of upwelling rate ( $W_0$ ) vs. maximum residual melt porosity ( $\phi$ ) showing contoured activity ratios for  $(^{230}\text{Th}/^{238}\text{U})$  (top panel),  $(^{226}\text{Ra}/^{230}\text{Th})$  (middle panel), and  $(^{231}\text{Pa}/^{235}\text{U})$  (bottom panel).

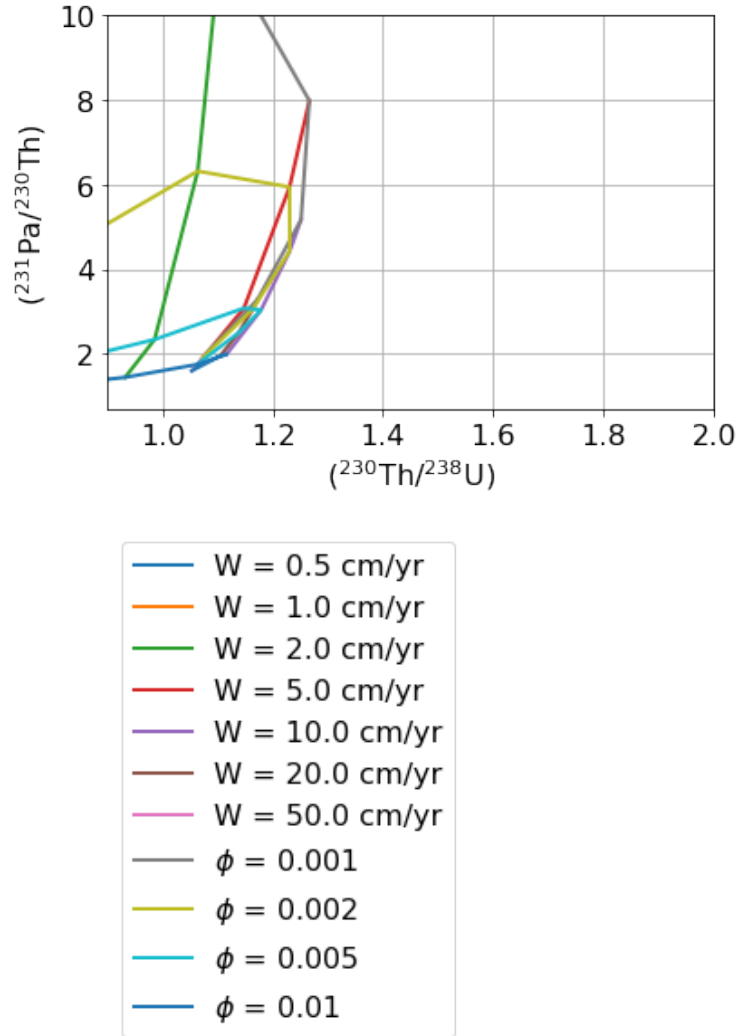
[34] : UserCalc.plot\_mesh\_Ra(Th,Ra,W0,phi0)  
604



605

[35]: UserCalc.plot\_mesh\_Pa(Th,Pa,W0,phi0)

606



607

608 **Figure 11.** Diagrams showing  $(^{226}\text{Ra}/^{230}\text{Th})$  vs.  $(^{230}\text{Th}/^{238}\text{U})$  (top) and  $(^{231}\text{Pa}/^{235}\text{U})$  vs.  
 609  $(^{230}\text{Th}/^{238}\text{U})$  (bottom) for the gridded upwelling rate ( $W_0$ ) and maximum residual porosity  
 610 ( $\phi$ ) values defined above.

## 611 4 Summary

612 We present pyUserCalc, an expanded, publicly available, open-source version of the UserCalc  
 613 code for determining U-series disequilibria generated in basalts by one-dimensional, decompression  
 614 partial melting. The model has been developed from conservation of mass equations with  
 615 two-phase (solid and liquid) porous flow and permeability governed by Darcy's Law. The model  
 616 reproduces the functionality of the original UserCalc equilibrium porous flow calculator (Spiegel-  
 617 man, 2000) in pure Python code, and implements a new disequilibrium transport model. The  
 618 disequilibrium transport code includes reactivity rate-limited chemical equilibration calculations  
 619 controlled by a Damköhler number,  $Da$ . For stable elements with decay constants equal to zero,  
 620 the equilibrium model reduces to batch melting and the disequilibrium transport model with  $Da$   
 621 = 0 to pure fractional melting. The method presented here can be extended to other applications  
 622 in geochemical porous flow calculations in future work.

## Acknowledgments

We thank K.W.W. Sims and P. Kelemen for initiating early discussions about creating a new porous flow disequilibrium transport calculator back in 2008. We also thank M. Ghiorso for inviting L. Elkins to join the ENKI working group and thereby catalyzing this fresh effort, and we further thank the working group for their helpful suggestions and feedback. L. Elkins received ENKI working group travel assistance that contributed to this research effort, and was supported by NSF award OCE-1658011.

## Data Availability Statement

The data set for this research consists of a code package, which is available in several ways: 1) in the supporting information, 2) through a binder container (at [https://mybinder.org/v2/gl/ENKI-portal%2FpyUsercalc/master?filepath=pyUserCalc\\_manuscript.ipynb](https://mybinder.org/v2/gl/ENKI-portal%2FpyUsercalc/master?filepath=pyUserCalc_manuscript.ipynb)), and 3) in the ENKI GitLab data repository (<https://gitlab.com/ENKI-portal/pyUsercalc>), which can also be accessed at the ENKI cloud server (<https://server.enki-portal.org/hub/login>) with a free GitLab account (register at <https://gitlab.com/ENKI-portal>).

## References

- Aharonov, E., J. A. Whitehead, P. Kelemen, and M. Spiegelman (1995), Channeling instability of upwelling melt in the mantle, *Journal of Geophysical Research: Solid Earth*, **100**(B10), 20433-20450.
- Bourdon, B., S. P. Turner, and N. M. Ribe (2005), Partial melting and upwelling rates beneath the Azores from a U-series isotope perspective, *Earth and Planetary Science Letters*, **239**, 42-56.
- Elkins, L. J., B. Bourdon, and S. Lambart (2019), Testing pyroxenite versus peridotite sources for marine basalts using U-series isotopes, *Lithos*, **332-333**, 226-244, doi: 210.1016/j.lithos.2019.1002.1011.
- Feineman, M. D., and D. J. DePaolo (2003), Steady-state  $^{226}\text{Ra}/^{230}\text{Th}$  disequilibrium in mantle minerals: implications for melt transport rates in island arcs, *Earth and Planetary Science Letters*, **215**(3-4), 339-355.
- Grose, C. J., and J. C. Afonso (2019), Chemical disequilibria, lithospheric thickness, and the source of ocean island basalts, *Journal of Petrology*, **60**(4), 755-790.
- Iwamori, H. (1993), Dynamic disequilibrium melting model with porous flow and diffusion-controlled chemical equilibration, *Earth and Planetary Science Letters*, **114**(2-3), 301-313.
- Iwamori, H. (1994),  $^{238}\text{U}$ - $^{230}\text{Th}$ - $^{226}\text{Ra}$  and  $^{235}\text{U}$ - $^{231}\text{Pa}$  disequilibria produced by mantle melting with porous and channel flows, *Earth and Planetary Science Letters*, **125**, 1-16.
- Jull, M., P. Kelemen, and K. Sims (2002), Consequences of diffuse and channelled porous melt migration on uranium series disequilibria., *Geochimica Et Cosmochimica Acta*, **66**, 4133-4148.
- Kogiso, T., M. M. Hirschmann, and P. W. Reiners (2004), Length scales of mantle heterogeneities and their relationship to ocean island basalt geochemistry, *Geochimica et Cosmochimica Acta*, **68**(2), 345-360.

- 660 Liang, Y., and B. Liu (2016), Simple models for disequilibrium fractional melting and batch melting  
661 with application to REE fractionation in abyssal peridotites, *Geochimica et Cosmochimica Acta*, **173**,  
662 181-197.
- 663 Lundstrom, C., J. Gill, and Q. Williams (2000), A geochemically consistent hypothesis for MORB  
664 generation, *Chemical Geology*, **162**(2), 105-126.
- 665 McKenzie, D. (1985), Th-230-U-238 Disequilibrium and the Melting Processes beneath Ridge Axes,  
666 *Earth and Planetary Science Letters*, **72**(2-3), 149-157.
- 667 Oliveira, B., J. C. Afonso, and R. Tilhac (2020), A disequilibrium reactive transport model for man-  
668 tle magmatism, *Journal of Petrology*, <https://doi.org/10.1093/petrology/egaa1067>.
- 669 Peate, D. W., and C. J. Hawkesworth (2005), U series disequilibria: insights into mantle melting  
670 and the timescales of magma differentiation, *Reviews of Geophysics*, **43**(1).
- 671 Qin, Z., F. Lu, and A. T. Anderson (1992), Diffusive reequilibration of melt and fluid inclusions,  
672 *American Mineralogist*, **77**(5-6), 565-576.
- 673 Shaw, D. M. (1970), Trace element fractionation during anatexis, *Geochimica et Cosmochimica*  
674 *Acta*, **34**(2), 237-243.
- 675 Sims, K. W. W., D. J. DePaolo, M. T. Murrell, W. S. Baldrige, S. Goldstein, D. Clague, and M.  
676 Jull (1999), Porosity of the melting zone and variations in the solid mantle upwelling rate beneath  
677 Hawaii: Inferences from U-238-Th-230-Ra-226 and U-235-Pa-231 disequilibria, *Geochimica Et Cos-*  
678 *mochimica Acta*, **63**(23-24), 4119-4138.
- 679 Sims, K. W. W., et al. (2002), Chemical and isotopic constraints on the generation and transport of  
680 magma beneath the East Pacific Rise, *Geochimica Et Cosmochimica Acta*, **66**(19), 3481-3504.
- 681 Spiegelman, M. (2000), UserCalc: a web-based uranium series calculator for magma migration  
682 problems, *Geochemistry Geophysics Geosystems*, **1**(8), 1016.
- 683 Spiegelman, M., and P. Kenyon (1992), The requirements for chemical disequilibrium during  
684 magma migration, *Earth and Planetary Science Letters*, **109**(3-4), 611-620.
- 685 Spiegelman, M., and T. Elliott (1993), Consequences of Melt Transport for Uranium Series Dise-  
686 quilibrium in Young Lavas, *Earth and Planetary Science Letters*, **118**(1-4), 1-20.
- 687 Stracke, A., and B. Bourdon (2009), The importance of melt extraction for tracing mantle hetero-  
688 geneities, *Geochimica Et Cosmochimica Acta*, **73**, 218-238.
- 689 Stracke, A., A. Zindler, V. J. M. Salters, D. McKenzie, and K. Gronvold (2003), The dynamics of  
690 melting beneath Theistareykir, northern Iceland, *Geochemistry Geophysics Geosystems*, **4**, 8513.
- 691 Van Orman, J. A., T. L. Grove, and N. Shimizu (2002a), Diffusive fractionation of trace elements  
692 during production and transport of melting in the earth's upper mantle, *Earth and Planetary Science*  
693 *Letters*, **198**, 93-112.
- 694 Van Orman, J. A., A. E. Saal, B. Bourdon, and E. H. Hauri (2006), Diffusive fractionation of U-series  
695 radionuclides during mantle melting and shallow-level melt-cumulate interaction, *Geochimica et*  
696 *Cosmochimica Acta*, **70**(18), 4797-4812.
- 697 Zou, H., and A. Zindler (2000), Theoretical studies of <sup>238</sup>U-<sup>230</sup>Th-<sup>226</sup>Ra and <sup>235</sup>U-<sup>231</sup>Pa dis-  
698 equilibria in young lavas produced by mantle melting, *Geochimica et Cosmochimica Acta*, **64**(10),  
699 1809-1817.